DOI 10.1007/s11237-021-09666-6
Theoretical and Experimental Chemistry, Vol. 56, No. 6, January, 2021 (Ukrainian Original Vol. 56, No. 6, November-December, 2020)

PREPARATION AND PROPERTIES OF FILMS OF ORGANIC-INORGANIC PEROVSKITES $MAPbX_3$ (MA = CH_3NH_3; X = Cl, Br, I) FOR SOLAR CELLS: A REVIEW

A. G. Belous,[1] A. A. Ishchenko,[2] O. I. V'yunov,[1] and P. V. Torchyniuk[1]

UDC 64.39.39:61.31.39.29:547.97:621.016.36

The latest results in the field of design of and research on organic-inorganic perovskites are summarized. The influence of chemical and physical factors, in particular the ratio of starting reagents, such as solvents, including polymers, temperature, and light radiation, on the formation of perovskite films and the features of their crystal structure are considered. The ways to increase the efficiency of film solar cells on the basis of such materials, as well as the possibility of creating composite materials using perovskites and organic dyes, are analyzed. The possibilities of using such systems are discussed.

Keywords: *organic-inorganic perovskites, organic dyes, hybrid structures, film synthesis, stabilization methods, spectral-luminescent properties, solar power conversion efficiency.*

INTRODUCTION

Currently, the worldwide electricity consumption is estimated at about 16 thousand TW·h. According to the experts, the demand for electricity by 2050 will increase to 30 thousand TW·h. Therefore, intensive research is being conducted to develop new energy sources, as traditional approaches to energy production, which are associated with the combustion of fossil fuels (oil, gas, coal), will not be able to meet all energy needs. In addition, the use of traditional energy sources leads to significant pollution of the environment and this can put humanity on the brink of survival. Solar energy is the most promising and efficient among various energy sources due to its unlimited amount and relatively small negative impact on the environment. Therefore, the use of photovoltaic solar cells (PV) is promising for electricity generation because they directly convert sunlight into electricity. In 1839, Edmond Becquerel was the first to convert sunlight into electricity. In 1905, Albert Einstein developed the theory of the photoelectric effect, for which he later received the Nobel Prize. The photovoltaic industry was created in 1954, when a solar cell was developed on the basis of crystalline silicon in the laboratory of Bell (USA) [1]. Over time, the second-generation solar cells based on A^3B^5 compounds (GaAs, CdTe, InP) were developed [2]. In the early 1990s, the third generation of dye-sensitized solar cells was developed [3]. Currently, the organic-inorganic perovskite-based solar cells (PSC, perovskite solar cell) are of considerable scientific and practical interest.

[1]V. I. Vernadsky Institute of General and Inorganic Chemistry, NAS of Ukraine, Kyiv, Ukraine. E-mail: belous@ionc.kiev.ua.
[2]Institute of Organic Chemistry, NAS of Ukraine, Kyiv, Ukraine. E-mail: al.al.ishchenko@gmail.com.

Translated from Teoretychna ta Eksperymentalna Khimiya, Vol. 56, No. 6, pp. 333-357, November-December, 2020. Received September 16, 2020; accepted November 16, 2020.

It should be noted that there are many materials based on complex oxides that crystallize in the structure of ABO_3 perovskite. They have played an important role in the chemistry of materials and the physics of condensed systems over the past few decades. The perovskites based on oxide system are characterized by various properties and are widely used in engineering, in particular in the development of ceramic capacitors [4], nonlinear materials [5], piezoelectrics [6, 7], high-temperature superconductors [8], giant magnetoresistance materials [9, 10], ionic conductors [11], high-quality ultrahigh-frequency dielectrics [12], and multiferroics [13]. Recent studies have shown that organic-inorganic perovskites are considered as potential materials for the creation of thin-film solar cells [14].

The $MAPbX_3$ organic-inorganic perovskites ($MA = CH_3NH_3$; X = Cl, Br, I) were synthesized in the 1980s [15, 16]. However, their physical and chemical properties were not studied at that time and the possibility of their practical use was unknown [17, 18]. For the first time in 2009, the authors of [19] studied hybrid perovskites as light absorbers in solar cells, the efficiency of which did not exceed 4%. In this work, the $MARbI_3$ hybrid perovskites are used as alternative dyes in the solar energy conversion cell using liquid electrolyte.

In 2012, several research teams simultaneously reported the creation of solid-state solar cells based on organic-inorganic perovskite, which demonstrate power conversion efficiency of 10-11% [20-22]. Since then, the organic-inorganic perovskites have attracted considerable scientific interest. They are characterized by a number of advantages; in particular, they can be synthesized using relatively simple and inexpensive technology and can be obtained on a flexible basis. The great potential of perovskite-based solar cells is confirmed by the fact that the power conversion efficiency (PCE) has increased from 3% to 25.2% (and to 28% in tandem architecture) in 10 years [19, 23]. Despite these advantages, such cells have disadvantages such as low stability and short uptime, which creates significant obstacles to their commercialization. The perovskite materials used in the solar cell can serve as both an absorption layer and an effective layer for charge transfer [24]. They are characterized by a high level of properties, which allows them to be considered as promising materials for the PV technologies of next-generation: high electron mobility (800 $cm^2/V^{-1}\cdot s^{-1}$) [25], long carrier diffusion length (more than 1 μm) [26, 27], ambipolar nature of moving charges [28], and high absorption coefficient (greater than 10^5 cm^{-1}) [26], etc.

Currently, a number of reviews have been published on the study of the $MAPbX_3$-based organic-inorganic perovskites ($MA = CH_3NH_3$; X = Cl, Br, I) [29-32]. However, they have relatively little data on phase transformations (intermediate phases) in the synthesis of perovskite films and the influence of solvent type on these processes, which is important in the development of film technology. There are no studies that consider the possibility of creating composite structures based on perovskites and organic dyes and their properties. Therefore, this review analyzes the features of the structure of organic-inorganic perovskite films, the methods of their synthesis, the influence of the ratio of starting reagents and the type of solvents on the formation of films, as well as the ways to increase their stability. The possible approaches to increase the efficiency of solar cells by creating hybrid structures based on perovskites and organic dyes, as well as architectural aspects of perovskite solar cells, are considered.

STRUCTURE OF $MAPbX_3$ ORGANIC-INORGANIC PEROVSKITES ($MA = CH_3NH_3$; X = Cl, Br, I)

The organic-inorganic perovskite-based materials have a crystalline structure similar to calcium titanate ($CaTiO_3$). The structure corresponds to the general formula ABX_3, where X is usually oxygen, nitrogen, carbon or halogen. There are two types of halide perovskites: alkali halide-based perovskite and organic-inorganic halide-based perovskite. The alkaline halide-based perovskite consists of a monovalent alkali cation (A) in the form of Cs^+, Rb^+, K^+, Na^+, and Li^+, a divalent cation (B) such as Pb^{2+}, Sn^{2+}, and Ge^{2+}, and halogen anions (X) such as Cl^-, Br^-, I^-, and F^-. The organic-inorganic halide-based perovskite has an organic monovalent cation (A) such as $CH_3NH_3^+$, $CH_3CH_2NH^+$, and $NH_2CHNH_2^+$ [33]. The A ion has coordinates (0.0, 0.0, 0.0) in the crystal coordinate system, and the B ion has coordinates (0.5, 0.5, 0.5). The size of A is usually larger than B, and the X ion is an anion with coordinates (0.5, 0.5, 0) [34].

The structure of the ABX_3 perovskite type is formed by BX_6 octahedra connected by vertices. The connection of octahedra occurs in such a way that it is possible to allocate rectilinear parallel octahedra chains on all three mutually perpendicular axes. The A cations are located in the space between the octahedra. Thus, if the B cations are surrounded by six X

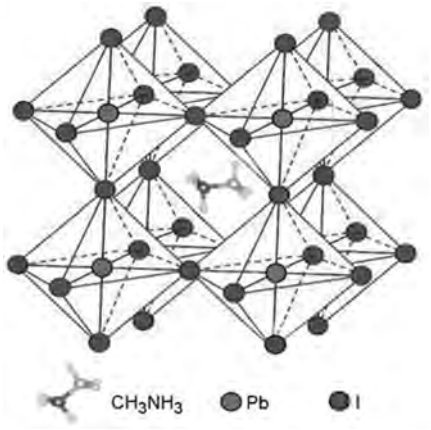

Fig. 1. The crystal structure of the perovskite type.

atoms, then the A ions, which occupy the center of the cuboctahedron, are surrounded by 12 anions. The X anion is surrounded by six cations, the four A cations lying at a distance $a/\sqrt{2}$ (where a is the parameter of the crystal cubic lattice) at the vertices of the square whose center is the anion, and the two B cations lying at a distance in the direction perpendicular to the square of the A ions [35].

It is necessary to fulfill two geometrical conditions that provide a dense packing of atoms and determine the allowable sizes of the A and B cations, and anions to provide the existence of the ABX_3 compounds of the perovskite structural type [36]:

$$R_B > 0.41R_X,$$

$$t_1 < t = \frac{R_A + R_X}{\sqrt{2}(R_B + R_X)} < t_2,$$

where R_B and R_X are approximate ionic radii with coordination number (CN) 6 and 12, respectively ($R_{CN=12} = 1.12R_{CN=6}$). The value of t (tolerance factor) is in the range of $t_1 \approx 0.764$; $t_2 \approx 1.03$.

The general chemical formula of complex perovskites can be represented as the following [37]:

$$(A'_{x_1} A''_{x_2} \ldots A^{i}_{x_i} \ldots A^{k}_{x_k})(B'_{y_1} B''_{y_2} \ldots B^{j}_{y_j} \ldots B^{l}_{y_l})X_3,$$

where $\sum_{i=1}^{l} x_i = 1$; $\sum_{j=1}^{l} y_j = 1$ ($x_i > 0$; $y_j > 0$).

Also the conditions of electroneutrality must be met in the formation of the perovskite structure:

$$\sum_{i=1}^{k} x_i n_A(i) + \sum_{j=1}^{l} y_j n_B(j) + 3n_X = 0,$$

where $n_A(i)$, $n_B(j)$, and n_X is the valence of the corresponding ions.

The organic-inorganic perovskites are characterized by a number of structural features; in particular, $CH_3NH_3PbI_3$ has a cubic structure ($Pm3m$ space group, $z = 1$) at temperatures above 327.2 K [16]. A phase transition of $CH_3NH_3PbI_3$ perovskite from the cubic structure to the tetragonal (space group $I4/mcm$, $z = 4$) is observed as the temperature decreases [38], and then it passes into the orthorhombic structure (space group $P222_1$) when the temperature is below 162.2 K [39]. Iodine ions form octahedra in this structure, inside of which there is a lead ion, which are interconnected by vertices along the x, y, z axes. $CH_3NH_3^+$ ions are located in the space formed by iodine octahedra. Taking into account that octahedra are large in size (compared to

oxygen octahedra in oxygen-containing perovskites such as $CaTiO_3$), $CH_3NH_3^+$ ions can move freely in their structure positions [38]. It should be noted that there is a certain disorder in the arrangement of CH_3 ions, which was studied in detail on single crystals by the authors of [38].

The most common absorbent material used for PSC is methylammonium lead trihalide ($MAPbX_3$, where X is a halide, which may be Cl, Br, or I). The parameters of a single cell increase from 5.68 to 5.92 to 6.27 Å with increasing size of the halide atom from Cl to Br, and to I. The problem of determining the tolerance factor in the organic-inorganic compounds is to estimate the ionic radii of molecular ions. This was solved by Kapustinskii and Yatsimirskii in the 1940s for molecular anions. The effective ionic radii of organic-inorganic perovskites with a molecular cation were determined by the authors [42]. In particular, the effective radius of methylammonium is 2.17 Å. Taking into account that $R_{Pb^{2+}_{CN=12}} = 1.49$ Å and $R_{I^{2+}_{CN=6}} = 2.2$ Å, the tolerance factor for $CH_3NH_3PbI_3$ is 0.837, which indicates the formation of a dense package of perovskite structure.

The band gap of methylammonium lead halide is usually in the range of 1.5-2.3 eV. $MAPbI_3$ is a direct-band material with a band gap of approximately 1.55 eV, while $MAPbBr_3$ and $MAPbCl_3$ have a relatively wider band gap of 1.8 and 2.3 eV, respectively. $FAPbI_3$ (where FA is formamidinium) shows a relatively narrow band gap of 1.48 eV, which indicates a larger current generation when using it as an absorbing layer, but this material showed less resistance. The use of smaller Cl^-, Br^- halides instead of I^- reduces the lattice constant, as a result of which the perovskite passes into a more stable cubic phase [22].

PECULIARITIES OF SYNTHESIS OF ORGANIC-INORGANIC PEROVSKITES

Obtaining organic-inorganic perovskite films is an extremely important problem because they can be used in the form of a film in the development of various optical systems and solar energy conversion cells. Currently, there are many synthesis methods of laboratory samples of perovskite films, including single-step deposition, two-step sequential deposition, fast deposition-crystallization, Lewis acid–base adduct approach for lead(II) iodide, treatment of vapor-containing solutions, thermal evaporation, pulsed laser spraying, and electrospray deposition.

The essence of the one-step synthesis method of the organic-inorganic perovskite films is to obtain a film directly from a salt solution using spin-coating or tape-casting [43-45]. There are two key points in this method: solvent evaporation and crystallization. The solvent evaporation and crystallization occur simultaneously in the traditional one-step method. This is not important during the deposition of perovskite films to the mesoporous structure [43, 44]. There is information about obtaining films using a single-step method when the synthesis is carried out under certain conditions: the crystallization process is slowed down at the beginning, and a smooth precursor film is formed with the subsequent formation of an organic-inorganic perovskite film by slow crystallization [46].

A perovskite film was obtained by means of rapid crystallization by accelerating the process of perovskite nucleation and crystallization before the solvent evaporation was completed [47, 48, 49].

The starting reagents (usually MAX, where X = Cl, Br, I, and PbI_2) are dissolved in different solvents to obtain the organic-inorganic perovskite films. The main solvents that are widely used for perovskites include N,N-dimethylformamide (DMF), γ-butyrolactone (GBL), and dimethyl sulfoxide (DMSO). It is known that the perovskite film obtained using DMF and GBL solvents is characterized by a low-quality surface, which is associated with the formation of perovskite with a short annealing time [33]. The DMSO solvent, which is able to form DMSO-PbI_2 complexes, is often used to slow down crystallization and improve the surface of perovskite [46, 50].

Various factors are involved in the process of obtaining films with higher PCE values: annealing temperature and annealing atmosphere. However, in some cases the literature data contradict each other. On the one hand, the synthesis of the organic-inorganic films in the absence of moisture allows one to obtain homogeneous continuous films with PCE = 11.4% [51]. On the other hand, a low level of moisture promotes the formation of a film with PCE = 17.1% and a filling factor FF = 80% [52, 53].

The $PbCl_2$ and MAI reagents in a ratio of 1:3 are often used to obtain films [21, 54-56]. A film with a wide grain size distribution of approximately 100-1000 nm was obtained in the study [21]. It is known that the formation of a uniform texture with a narrow grain size distribution for organic-inorganic perovskite is possible when using annealing at 130°C [57].

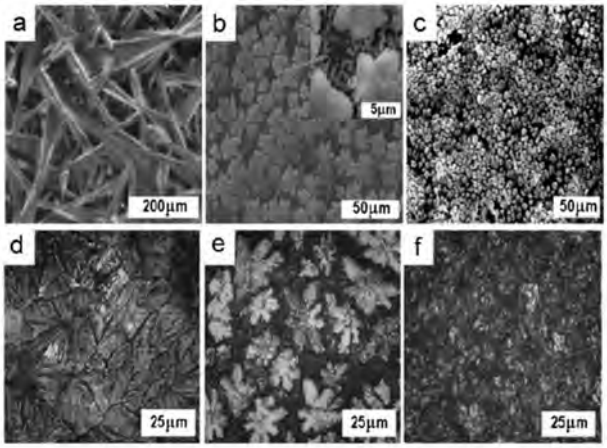

Fig. 2. The image of the surface of the $CH_3NH_3PbI_3$ perovskite films obtained using DMF (a-c) and DMSO (d-f) solvents at different ratios of the PbI_2 and CH_3NH_3I starting reagents: 1:1 (a and d); 1:2 (b and e); 1:3 (c and f). The data were partially used in the study [71] with the permission of the Institute of General and Inorganic Chemistry, NAS of Ukraine, under Creative Commons Attribution 4.0 International (CC BY 4.0) License http://creativecommons.org/licenses/by/4.0/.

Various additives are used to optimize the morphology and increase the stability of perovskites, such as organic ammonium salts, in particular methylammonium chloride (MACl), which is able to influence the formation of the perovskite film [58]. The use of MACl helps to improve the performance of solar cells. The MAI·PbI_2·MACl intermediate compound is formed in the perovskite films when the MACl content is increased, which slows down the crystallization. It is known that other ammonium salts can be used to control the morphology of the film: ammonium chloride [59], guanidinium iodide [60], methylammonium thiocyanate [61], ammonium thiocyanate [62], and ammonium acetate [63].

1,8-Diiodooctane (DIO) can also be used as an additive, which improves the morphology of the organic-inorganic perovskite films [64, 65]. DIO slows down the crystallization rate of the perovskite structure due to the formation of chelate complexes with Pb^{2+} [65].

The nature of lead salts ($PbCl_2$, $Pb(NO_3)_2$, $PbCO_3$) can affect the morphological properties of the organic-inorganic perovskites [66, 67]. It was possible to obtain the smoothest surface of the film when using $Pb(CH_3COO)_2$ with 3MAI [68]. Different lead salts can significantly affect the growth of crystals in the process of obtaining a film, which is associated with a change in the activation energy required for the transition of the precursor to perovskite [69].

It has been shown that a homogeneous perovskite film with a large crystal size can be obtained by single-step deposition using $Pb(CH_3COO)_2$ and thiosemicarbazide additive. A cell with 1.025 cm^2 area, obtained on the basis of this film, shows a PCE of 19.19% [70].

The authors of [61, 62, 71] studied the effect of the solvent type (DMF, DMSO) and the ratio (1:1; 1:2; 1:3) of the starting reagents (PbX_2 and MAI) on the phase transitions that occur during the formation of the crystal structure of $CH_3NH_3PbI_{3-x}X_x$ perovskite, on the morphology of the films, as well as on their stability under the effect of moisture and radiation. The studies [71, 72] showed that regardless of the ratio of the starting reagents, a perovskite structure is formed after heat treatment when using DMF solvent. Different intermediate phases are formed depending on the ratio of the starting reagents. In particular, the intermediate phases are $(CH_3NH_3)_2(DMF)_xPbI_4$, $(CH_3NH_3)_3(DMF)PbI_5$, and $(CH_3NH_3)_2(DMF)_2Pb_3I_8$ at a ratio of the PbI_2 and MAI starting reagents of 1:1, and $(CH_3NH_3)_2(DMF)_xPbI_4$, $(CH_3NH_3)_3(DMF)PbI_5$, $(CH_3NH_3)_2(DMF)_2Pb_2I_6$, and $(CH_3NH_3)_2(DMF)_2Pb_3I_8$ at a ratio of 1:2, whereas the intermediate phases $(CH_3NH_3)_2(DMF)_xPbI_4$ and $(CH_3NH_3)_3(DMF)PbI_5$ are formed at a ratio of 1:3. It is important that the morphology of the film, which was formed on a smooth glass surface, changed significantly with the change in the ratio of the starting reagents (Fig. 2a, b, and c) [62]. It is shown that the stability of perovskite films can be improved by using a layer of a polyvinyl butyral-based protective polymer [71] (Fig. 3). The stability of the films was evaluated by the content of the PbI_2 phase, which

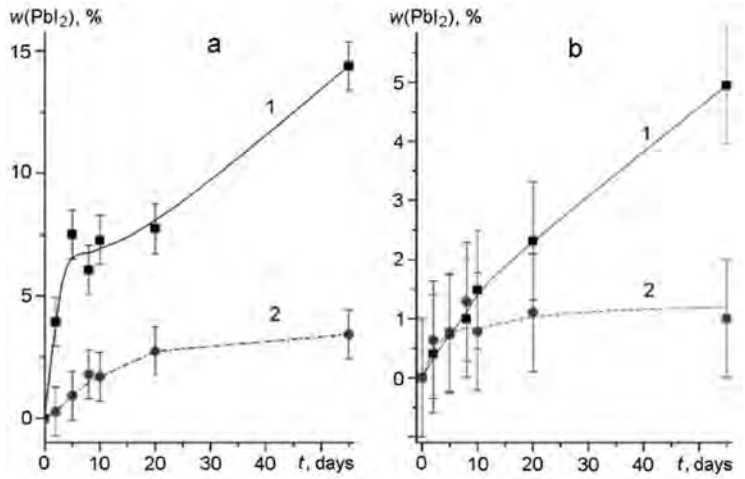

Fig. 3. The content dependence of the PbI_2 phase, which is formed during the decomposition of the organic-inorganic perovskites films in air without additives (a) and with the addition of 5% polymer (b) with different ratios of the starting reagents in air: *1*) 1:1; *2*) 1:3. Submitted according to the study data [71] with the permission of the Institute of General and Inorganic Chemistry, NAS of Ukraine, under Creative Commons Attribution 4.0 International (CC BY 4.0) License http://creativecommons.org/licenses/by/4.0/.

is formed as a result of the continuous degradation of the organic-inorganic perovskite film (Fig. 3). The organic-inorganic perovskite films, obtained at a ratio of the starting reagents of 1:1, decompose under a 55-day influence of moisture to form a PbI_2 phase, the content of which is 14% (Fig. 3a). However, the content of the PbI_2 phase is much lower and amounts to 3.5% for the films obtained at a ratio of 1:3. Therefore, the stability of the organic-inorganic perovskite films depends on the ratio of the starting reagents in the synthesis process. The perovskite films are the most stable at a ratio of 1:3. It was found that the PbI_2 content is much lower and the stability of the perovskite films with polymer is higher. The content of PbI_2 was 5 and 1%, respectively, in the perovskite films obtained at a ratio of the starting reagents of 1:1 and 1:3 with the addition of polyvinyl butyral (Fig. 3b). It was possible to increase the resistance of the $CH_3NH_3PbI_3$ organic-inorganic perovskite films to moisture when using polymer.

A number of differences were observed when using DMSO solvent compared to DMF solvent [73]. In particular, regardless of the heat treatment temperature, the perovskite film contained insignificant concentrations of ($(CH_3NH_3)_2(DMSO)_2Pb_3I_8$, PbI_2.DMSO) impurity phases at a ratio of the starting reagents of 1:1. It is possible to obtain a single-phase perovskite structure when the ratio of the starting reagents is 1:2 and 1:3. Depending on the ratio of the starting reagents, the perovskite structure is formed through a number of intermediate phases when using DMSO as a solvent. The intermediate phases are $(CH_3NH_3)_2(DMSO)_xPbI_4$, $(CH_3NH_3)_2(DMSO)_2Pb_3I_8$, $PbI_2{\cdot}2DMSO$, and $PbI_2{\cdot}DMSO$ at a ratio of 1:1, $(CH_3NH_3)_2(DMSO)_xPbI_4$, $(CH_3NH_3)_2(DMSO)_2Pb_3I_8$, $PbI_2{\cdot}2DMSO$, and $PbI_2{\cdot}DMSO$ at a ratio of 1:2, while the $(CH_3NH_3)_2(DMSO)_xPbI_4$, $(CH_3NH_3)_2(DMSO)_2Pb_3I_8$, $PbI_2{\cdot}2DMSO$, and $PbI_2{\cdot}DMSO$ intermediate phases are formed at a ratio of 1:3. The morphology of the films is significantly affected by the ratio of the starting reagents, which is similar to the case of DMF solvent (Fig. 2d, e, and f). It is important to note that the films synthesized from the DMSO solutions show greater stability to irradiation when compared to DMF (Fig. 4).

It was found out that regardless of the ratio of the starting reagents (1:2, 1:3), the fluorescence intensity of the perovskite films obtained using DMF as a solvent gradually changes over time [71], which is most likely due to further changes in its morphology (Fig. 4, curves 1 and 3). The fluorescence intensity of the corresponding films obtained using DMSO under similar conditions remains almost constant, which indicates their much higher stability (Fig. 4, curves 2 and 4).

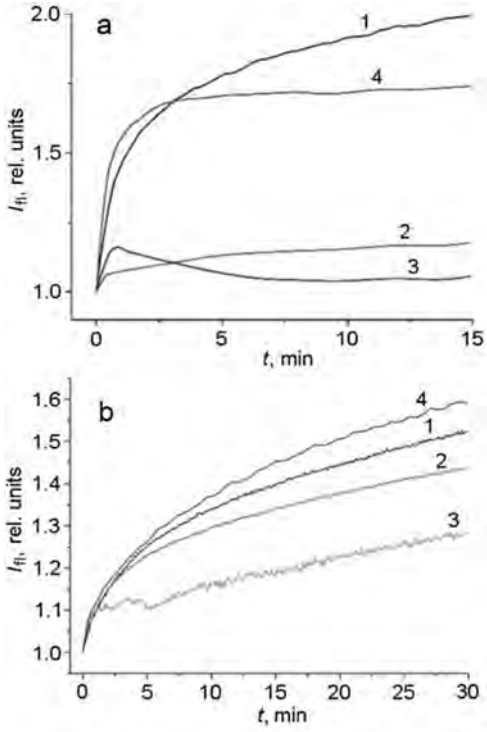

Fig. 4. The dependence of the fluorescence intensity I_{fl} (excitation wavelength 470 nm) on the irradiation time of the organic-inorganic perovskite films obtained from the solution: a) DMF (1 and 3) and DMSO (2 and 4) with a ratio of the starting reagents 1:2 (1 and 2) and 1:3 (3 and 4); b) DMF with a ratio of the starting reagents 1:1 (1 and 2) and 1:3 (3 and 4) without additives (1 and 3) and with the addition of 5% polymer (2 and 4).

These results indicate the importance of studying the conditions of crystal structure formation in the organic-inorganic perovskites depending on the nature and ratio of the initial components, as well as the type of solvent, which is necessary to develop methods of increasing the stability of perovskite films against the influence of external factors.

Apart from different approaches aimed at delaying the crystallization process, other approaches are also used to obtain organic-inorganic perovskites films with a high-quality surface. There are data on the use of fast crystallization or deposition of the film from a solvent. The authors of [47, 48] demonstrated a successful technology of preparation of homogeneous perovskite films, which allowed them to obtain solar cells with a high coefficient of solar energy conversion (~17.9%) and without hysteresis on the current-voltage dependences. The essence of this approach is that a high-uniformity film precursor with DMSO as a complex used to delay the perovskite crystallization is obtained at first, which required a short annealing. In contrast, the authors of [74, 75] developed an insoluble concept (the fast crystallization-deposition method). The key point is the deposition of an antisolvent during spin-coating to obtain a uniform film. This solvent does not dissolve the perovskite precursor film but only mixes with the solvent used in the synthesis. This leads to a sharp increase in the concentration of the material of the perovskite precursor and to the fast deposition of the perovskite film over the entire surface of the supporter. It is possible to obtain a homogeneous perovskite film with larger crystal grains [24]. Chlorobenzene, benzonitrile, ethanol, benzene, xylene, methanol, ethylene glycol, toluene, and acetonitrile are used as antisolvents.

The studies [76, 77] showed the influence of the ratio of the PbI_2 and MAI starting reagents (1:1, 1:2, and 1:3) on the formation of the perovskite structure and the microstructure of the films deposited on a smooth surface (glass). Depending on

the ratio of the starting reagents and the heat treatment temperature, the formed films may contain other intermediates apart from $CH_3NH_3PbI_3$ perovskite.

Mitzi, et al. proposed a two-step deposition method to avoid the disadvantages of the perovskite film preparation when using the one-step method [78].

At first, the authors [78] obtained a PbI_2 film, which was then immersed in a methylammonium iodide (MAI) solution to obtain a perovskite film by a two-step method. Homogeneous perovskite films with strong photoluminescence were obtained. Obtaining a PbI_2 film is possible using solutions for synthesis or vacuum deposition. It was possible to obtain films that showed a power conversion efficiency of >14% by using this method [79]. The two-step method of obtaining organic-inorganic perovskite films is often used for the manufacture of highly efficient solar cells [80-82]. It is necessary to consider the diffusion rate of MAI in the PbI_2 film in the two-step method, while the morphology of the final film is mostly determined by the characteristics of the PbI_2 film. The PbI_2 film is deposited on a warm supporter (60-70°C) using spin-coating to obtain a smooth perovskite film [79-83]. Films with better perovskite morphology are obtained by the two-step method in comparison with the one-step solution deposition. It is possible to deposit the large grain thin perovskite films by changing the concentration of MAI, but the disadvantage includes a low-quality surface coating and incomplete conversion of PbI_2 to perovskite [84]. It should be noted that the use of a mesoporous structure, on which the film is deposited, allows one to obtain perovskite films in a short time (15 s) [79]. However, problems arise when smooth surfaces are used for the film coating. A perovskite film with PCE of 17.67% was obtained by the two-step deposition method using 3,3,5,5-azobenzene tetracarboxylic acid additive. The PSC based on it retains 84% of the initial PCE for 30 days [85].

Other methods of obtaining organic-inorganic perovskite films are also known. The authors of [86] used the Lewis acid–base adduct approach for lead(II) iodide when PbI_2 was dissolved in DMF, and a MAI equimolar solution was prepared in DMSO. The MAI·PbI_2·DMSO and PbI_2·DMSO adduct is formed by the reaction between PbI_2 Lewis acid and DMSO and/or iodine(I^-) Lewis base. This method allowed one to obtain a $MAPbI_3$ film and a solar cell based on it with a power conversion efficiency of 19.7% [87, 88]. For the first time, a vacuum-deposited $CH_3NH_3PbI_{3-x}Cl_x$ perovskite film was prepared by the simultaneous thermal evaporation of MAI and PbI_2 precursor salts from different sources at a pressure of 10^{-5} bar in a ratio of 4:1 [89].

Liang, et al. obtained a PbI_2 film using the pulse laser deposition method (PLD), on which MAI was deposited using the spin coating method. A compact, crystalline, homogeneous, continuous, and large grain size perovskite film was obtained after heat treatment [90].

Stable and moisture-resistant films and PSC, which poorly degrade in high humidity conditions, were obtained by the electrospray deposition [91].

An extraordinary effect has recently been discovered; in particular, light has a strong influence on the perovskite formation rate and the film morphology in both main deposition methods: sequential deposition and the antisolvent method [92]. Integrated white light LEDs were used as a radiation source, which simulated the spectrum and intensity of the solar radiation. The reaction of lead iodide with methylammonium iodide was studied using confocal laser scanning fluorescence microscopy and scanning electron microscopy. It is shown that the former crystallizes before the intercalation of the latter begins, with the formation of perovskite. Then a structural reorganization begins, as a result of which mixed crystals of PbI_2, in particular, perovskites, are formed [92]. It was found that the formation of perovskite by sequential deposition is significantly accelerated by light. The effect of light on morphology is reflected in the doubling of the efficiency of solar cells [92]. Contrary to the above data, it is shown that the best photoelectric parameters are achieved in the preparation of films in the dark by using the antisolvent method to form perovskite in the above one-step reaction with the same starting materials [92].

As a result of photoelectric studies at different temperatures and intensities of light fluxes, it was found that the efficiency of perovskite-based solar cells is not associated with the heating of samples under the influence of light but is determined by the probability of formation of electron-hole pairs under its action [92].

According to our observations, the perovskite formation rate is affected not only by integral light but also by monochromatic light (Fig. 4a and b). Thus, when studying the kinetics of luminescence attenuation of $CH_3NH_3PbI_3$ organic-inorganic perovskite obtained at a ratio of the starting reagents of 1:1 and 1:3, the luminescence intensity increased when excited by both visible radiation (470 nm) and UV (370 nm). Moreover, the effect of the former is greater than the latter, despite the fact that the energy of light is smaller at a wavelength of 470 nm than that of 370 nm. This can be explained by the fact that the wavelength of visible light falls to the region of much higher intensity of perovskite absorption than UV radiation

(Fig. 4b). The fluorescence intensity reaches a constant value only after 70-90 min, depending on the composition of the perovskite and the excitation wavelength. A similar effect was observed in the perovskite films with polymer (Fig. 4b, curves 2 and 4). This phenomenon can also be explained by the change in the morphology of the perovskite film due to crystallization processes under the influence of light. According to the study [93], the luminescence intensity of crystals is higher than the intensity of amorphous components.

The discovery of light-induced crystallization not only reveals a previously unknown tuning source of optoelectronic properties, but also new ways of intentional control of the morphology and structuring of perovskites for various applications.

A new method of $MAPbBr_3$ nanoparticle formation *in situ* in a polystyrene dispersion in toluene in the absence and in the presence of GAG:Ce@PS luminophore has been proposed [94, 95]. A uniform distribution of nanoparticles of perovskite and luminophore in the polymer matrix and a high quantum yield of photoluminescence (up to 90%) is achieved [95]. It is shown that its color can be controlled by means of nano-dimensional effects. The use of $MAPbBr_3$/GAG:Ce@PS nanocomposite films in white LEDs allows one to increase the color rendering rate [94].

The simple manufacturing methods and high electrical properties of organic-inorganic perovskites contribute to the successful application of PSC in practice. This requires the development of synthesis methods that would ensure the manufacture of large-area cells. The organic-inorganic perovskite films are made on a small area in the laboratory usually using "spin coating" for this purpose. However, this method cannot be used to obtain high-quality films on a large area. Therefore, other methods are being developed for the manufacture of large-area PSC (and perovskite films), in particular, inkjet printing, drop casting, doctor blade coating, slot-die coating, and spray coating.

The "inkjet printing" method was used for the first time to obtain perovskite films [82]. Inkjet printing technologies in PSC manufacture provided high resistance to moisture and heat [96].

The "drop casting" method is inexpensive, simple, characterized by high productivity, and is suitable for large-scale production [24].

The "doctor blade coating" method is also inexpensive and easy to perform. Yehao Deng et al. first used this technology to obtain PSC, which included indium tin oxide (ITO)/hole transport layer (HTL)/$MAPbI_3$/6,6-phenyl-C_{61}-butyric acid methyl ester ($PC_{60}BM$)/C_{60}/2,9-dimethyl-4,7-diphenyl-1,10-phenanthroline (BCP)/Al. The cell PCE reached 15.1% [97].

The "slot-die coating" was used by Verhees et al., which allows one to produce large-area panels of 12.5×13.5 cm with a 10% cell PCE [98].

"Spray coating" can also be used to obtain perovskite films of large area [99-101]. Depending on the drop spraying method on the supporter, this method is classified as follows: ultrasonic spraying (ultrasonic vibration), pneumatic spraying (fast gas flow), and electric spraying (electrostatic repulsive force) [102]. Barrow et al. used this method to produce a planar perovskite solar cell based on mixed halide perovskite ($CH_3NH_3PbI_{3-x}Cl_x$) and achieved a PCE of 11% [99].

ARCHITECTURE OF ORGANIC-INORGANIC PEROVSKITE-BASED SOLAR CELLS

In general, a perovskite-based solar cell contains five components: cathode, hole transport layer (HTL), absorber layer, electron transport layer (ETL), and transparent conductive oxide (TCO) (Fig. 5). The function of HTL is to collect holes in the sorbent layer, transport them to the cathode, and block electrons. Accordingly, the function of the electron transport layer is to collect electrons, transfer them to the anode, and block holes.

All components of the cell play an important role in obtaining stable and highly efficient PSC: ETL, HTL, perovskite, etc. [103].

The dye-sensitized solar cells invented by M. Grätzel were the predecessors of perovskite [3]. They have a similar design. The principle of their work is as follows. When sunlight is absorbed by an organic dye, an electron transitions from its HOMO to LUMO, from which it then moves to the conduction band at LUMO of the semiconductor (usually TiO_2) until it reaches the anode. As a result, a "hole" is formed on the dye, to which an electron migrates from I^- ions, which also receives an electron from the semiconductor and is converted into an I_3^- ion by transferring it to the cathode. Thus, there is a potential difference between the contacts.

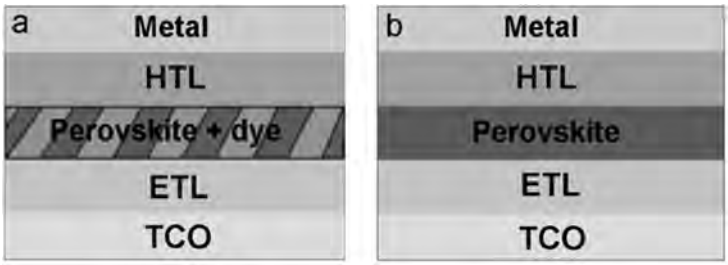

Fig. 5. The architecture of organic-inorganic perovskite-based solar cells, where organic-inorganic perovskite is used as a liquid electrolyte (a) and as a solid layer (b).

Simplicity and low manufacturing cost compared to silicon and GaAs have prompted numerous studies in this field [3, 104-106]. However, the low stability due to electrochemical processes, especially with "wet electrodes," still prevents their actual implementation [106]. The production of developed metal complexes based on ruthenium and organic ligands is expensive and time consuming [107]. In addition, a 30-year research on PCE of dye-sensitized solar cells (DSSC) invented by M. Grätzel shows that it practically does not exceed 13% [108].

It should also be mentioned that together with Grätzel's organic-inorganic photovoltaics, organic photovoltaics is developing rapidly. The role of hole and electron layer is performed by organic electron-donor and electron-acceptor molecules, respectively. Currently, the highest PCE of organic photovoltaic structures has reached 17.3% [110]. The conversion efficiency rate of solar energy into electricity is also low. However, the most likely difficulty in the further progress of organic photovoltaics will probably be associated with the research and development of new extraordinary chromophore systems. They will require a difficult multi-stage synthesis and high purification.

The progress in achieving light energy conversion efficiency is much higher after 10 years since the discovery of perovskites when compared to Grätzel's DSSC and organic photovoltaic structures for the last 30 years [108, 110, 111]. However, it should be noted that dyes are still unsurpassed sensitizers of various photoprocesses. Therefore, they are useful for hybrid light-sensitive materials, including perovskite-based, which will be analyzed below.

Currently, various HTL are used, in particular spiro-OMeTAD, NiO, CuO, CuI, and Cu_2O [112], etc. TiO_2, SnO_2, ZnO, CdSe, WO_3, $ZnSnO_4$, and $SrTiO_3$ [113], etc. are used as ETL. The transport layers should be characterized by good heat resistance, non-toxicity, and should be resistant to external degrading factors [114, 115, 116]. There are various constructions of perovskite-based solar cells, such as dye-sensitized structure, solid mesoscopic structure (Fig. 5), meso-superstructure, regular structure, planar *n-i-p* heterojunction structure, and inverted planar structure.

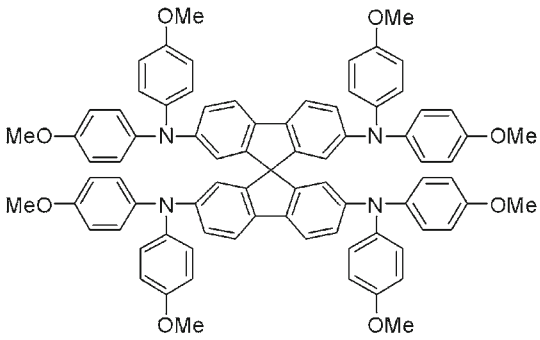

Spiro-OMeTAD

In 2009, the first PSC was manufactured by Kojima et al. [19]. They used the DSSC architecture, where transparent electrically conductive FTO glass (doped with SnO_2 fluorine) was used as a supporter on which a transparent layer of hole-blocking conductive oxide was deposited. A layer of TiO_2 (compact fine-grained (c-TiO_2) and mesoporous TiO_2 of micron thickness (m-TiO_2)) was used as HTL, on which a liquid $MAPbI_3$ electrolyte and $MAPbBr_3$ perovskite were deposited.

This PSC, where $MAPbI_3$ was the organic-inorganic perovskite, showed PCE = 3.81%. This device is no longer used due to its low stability and PCE, and the presence of liquid electrolyte.

The instability caused by the use of liquid electrolyte was overcome in 2012 [20]. Kim et al. reported the first solid-state solar cell that reached 9.7% PCE. This group used nanoparticles of precipitated m-TiO_2 with a micron thickness, which fill the pores of the spiro-OMeTAD hole transport material. This created a direct contact between the hole transport layer and the sensitizer, while the rest of the HTL served as a cover layer over m-TiO_2. The device showed higher efficiency, better stability, and worked for 500 h under continuous lighting.

Snaith proposed to change the structure of the device; in particular, m-TiO_2 was replaced by an insulating layer of m-Al_2O_3 (meso-superstructured PSC) [87]. The main purpose of this work was to study the behavior of electron transport through perovskite and to study the importance of m-TiO_2 in the PSC functionality. The result was unexpected, the transport of charge occurred at a higher rate, and the photocurrent increased. Their work showed that the charge was collected ten times faster using this device modification. The no-load voltage increased from 200 to 300 mV, thus increasing the PCE to 10.9%, open-circuit voltage V_{oc} = 0.98 V, FF = 63%, and short-circuit current J_{sc} = 17.8 mA/cm^2. In 2013, Ball et al. made PSC using an absorber based on a mixed $MAPbI_{3-x}Cl_x$ halide, which reduced the processing temperature from 500 to 150°C and achieved a PCE of 12.3 [117]. All the basic functions of solar cells have been achieved even after processing at low temperature: absorption, generation, and collection of carriers along with minimal recombination losses. This work showed that the metal oxide framework, which was deposited on perovskite, can be processed at low temperatures, which allows one to make PSC on a flexible supporter.

In 2013, Heo et al. proposed a configuration (regular structure) where m-TiO_2 pores are completely filled with $MAPbI_3$, forming $MAPbI_3$ columns. These columns were coated with thin polytriarylamine (PTAA) as a hole transport material (HTL) using an Au electrode. The device had PCE = 12%, V_{oc} = 0.997 V, FF = 72.7%, and J_{sc} = 16.5 mA/cm^2 [22].

The proposed "planar structure of the *n-i-p* heterojunction" is similar to thin-film solar cells based on perovskite. The structure of the device included a TCO cathode (transparent conductive oxide), *n*-type ETL, perovskite film, HTL/*p*-type, and a metal anode. This configuration excluded the mesoporous layer from the traditional structure of the organic-inorganic perovskite-based solar cell. In 2013, Snaith et al. proposed co-evaporation of $PbCl_2$ and MAI from two sources in order to improve the quality of the film. They deposited a $MAPbI_{3-x}Cl_x$ film on the c-TiO_2 layer, reaching PCE = 15%, V_{oc} = 1.07 V, FF = 67%, and J_{sc} = 21.5 mA/cm^2 [89]. In 2018, Yang et al. proposed a highly efficient *n-i-p* planar structure using EDTA of complex tin oxide (SnO_2) as ETL, $FAPbI_3$ as an absorbing layer with a small amount of Cs doping to improve phase stability, and spiro-OMeTAD as a hole transport layer (HTL), and achieved PCE = 21.6%, V_{oc} = 1.11 V, FF = 79.2%, and J_{sc} = 24.55 mA/cm^2 [118]. It is well known that although PSC with organic HTM achieves a fairly high initial PCE, they are subject to rapid degradation. PSC with inorganic HTM not only achieves a high PCE value but also shows relatively better device stability. The most stable behavior is shown by carbon-based HTM [119]. Xingyue et al. demonstrated carbon-based *n-i-p* planar PSC, which showed PCE 17.46%, J_{sc} = 22.41 mA/cm^2, FF = 0.726, and V_{oc} = 1.073 V. The device retained 97% of its initial efficiency for 1200 h [120].

Along with the *n-i-p* planar structure and the regular structure, PV researchers are developing *p-i-n* type solar planar cells. This configuration is usually called an inverted structure. It has an anode (TCO), *p*-type HTL, perovskite, *n*-type ETL, and a metal cathode. In 2018, Tang et al. developed a highly efficient inverted planar structure. The device reached a PCE of 15.47% [121].

Organohalide perovskites have excellent optoelectric properties at room temperature. The wide band gap provides light absorption in almost the entire visible spectrum and at the edge of the near-IR range of the spectrum. Therefore, photodiodes based on them have been successfully used [122]. Both wide- and narrow band types have been developed. However, due to the limited IR range of light absorption, photodiodes operating in the long-wavelength range of more than 1 μm cannot be implemented on organohalide perovskites. Therefore, the creation of hybrid light-sensitive materials, such as perovskite-organic dye, is considered as an important step [122-124]. These hybrids combine the best properties of each component: perovskite provides high mobility of charge carriers, and dye provides the required spectral range [122]. An important feature of such a composite is that its components, such as perovskite and dye, can be deposited in one layer, thus forming a heterojunction. Moreover, the process uses the same technology and the same solvent as in the manufacture of perovskite films. Another important aspect is that the organic dye in a certain range of concentrations does not change the crystal structure of perovskite and does not violate the homogeneity of the photoactive layer [122]. The absorption spectra of

the hybrid composite clearly show the absorption bands of the components. These bands are practically unchanged compared to the corresponding bands of individual dye and perovskite. This suggests that the components are not associated and do not form adducts with each other [125]. According to the study [126], this can be explained by the presence of a bulky substituent in the meso position of the polymethine chain and the hetero-residue of the $CyPF_6$ and $Cy1BF_4$ dyes used in the study [122]. Such substituents create steric hindrance to the convergence of monomer molecules.

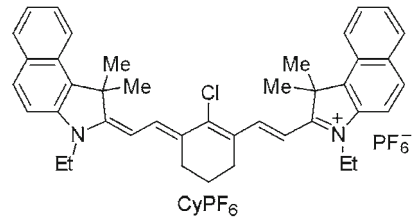

$CyPF_6$

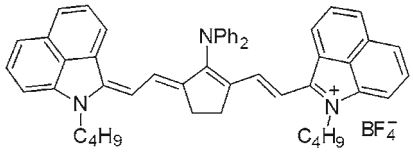

$Cy1BF_4$

It is necessary to take into account not only the absorption region, but also the ratio of the limit orbitals of dye and perovskite when choosing dyes for hybrid composites. The optimal condition suggests that the HOMO energy is higher in dye and LUMO is lower than in the corresponding perovskite orbitals. In this case, the hole will be transported from the last to the first, and the electron will be transported visa-versa [122]. Thus, segregation of electrons and holes is achieved, which leads to inhibition of the negative process of their recombination.

The $CyPF_6$ and $Cy1BF_4$ polymethine dyes correspond to the ratio of the orbitals described above [122]. In this case, the choice of polymethines is quite justified, since they have the highest extinctions and the widest spectral and luminescent range among organic dyes [127]. They achieved the highest π-π^* absorption region, that is, electron transition of 1.62 μm [128]. They have different structural variations (donor-acceptor properties of end groups, length of polymethine chromophore, electron asymmetry, nature of substituents, isomerism, the interaction of chromophores, etc.), which makes it possible to intentionally control the ratio of their limit orbitals and therefore photo- and electrophysical properties [122, 129, 130]. Additional optimization of the initial parameters of the hybrid composite, such as perovskite-organic dye, can be achieved by selecting the concentration of the latter [122].

The use of $CyPF_6$ and $Cy1BF_4$ polymethine dyes in this composite allows one to create broadband photodiodes with sensitivity in the entire visible and near IR range of the spectrum up to 1.6 μm at a satisfactory time, response frequency to the input light signal, and the signal-to-noise ratio [122]. They do not require cooling and can be used at room temperature as most infrared photodetectors.

The expansion of the perovskite sensitivity zone in the near IR range is a necessary condition for the creation of effective PSC. Therefore, hybrid structures of perovskite-polymethine dye are promising materials for this purpose [131].

$CyPF_6$ and $Cy1BF_4$ dyes belong to the ionic type. Despite the above advantages, like other ionic polymethines they can have a potential disadvantage, such as the occurrence of dark currents due to ion drift [132]. Therefore, it is desirable to develop intraionic dyes that do not contain free counterions for the newest photodetectors. The most promising should be squaraines, croconates, and merocyanines among such dyes. We have synthesized the first representatives of all these compounds with intense absorption in the region of 1 μm [133, 134].

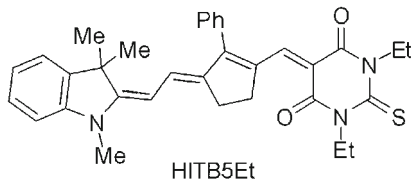

HITB5Et

The study [135] described the HITB5Et intraionic (merocyanine) dye, which is fragmentarily similar to the $CyPF_6$ ionic polymethine. Due to the selection of donor-acceptor properties of end groups and length and structure of the polymethine chain, its electronic structure is as close as possible to the state of ideal polymethine [136]. The highest intensity of absorption and the deepest color is achieved for this state, which is comparable with the corresponding characteristics of ionic dyes. Thus, absorbing light in the same range as the $CyPF_6$ dye, it has almost the same extinction as the latter. Due to the mentioned spectral properties and the absence of dark currents, HITB5Et merocyanine has been successfully used as a sensitizer in the photoactive layers of organic solar cells with a heterojunction [135, 137].

Thus, summarizing the features of merocyanines, it should be expected that their use in hybrid semiconductors, such as perovskite-merocyanine, in contrast to ionic dyes, will not only expand the sensitivity range in the IR region of the spectrum but also provide such hybrids with new functionality.

INSTABILITY OF SOLAR CELLS BASED ON ORGANIC-INORGANIC PEROVSKITE FILM

The main operational disadvantage of perovskites is their low stability [138-143]. The best laboratory samples of perovskite-based solar cells show properties that are not inferior to the efficiency of silicon solar cells, but they are characterized by instability to various external factors: moisture, oxygen, temperature, light, etc. [144]. It should be noted that the uptime of silicon photocells reaches 25 years, while perovskite-based cells have a much shorter lifespan, from a few days to months and a maximum of up to a year [145]. The PSC contact with moisture and oxygen can be avoided by using PSC encapsulation [146-148]. Encapsulation increases the total cost of the device and cannot protect the device from the harmful effects of other factors such as lighting, displacement, and heat [149]. The electrical displacement in the case of a *p-n* junction occurs upon application of an external voltage. There are direct and reverse (or shut-off) displacements. In the first case, a positive potential is created in the *p*-type region, a negative potential is created in the *n*-type region (a field of the same direction with a junction field), and the opposite in the second case [150].

Aqueous solutions of HI, solid PbI_2, and volatile CH_3NH_2 are formed when the perovskite film interacts with water and oxygen molecules [151, 152]. Instability under the effect of moisture usually occurs due to the hygroscopic nature of amine salts. This leads to the formation of products similar to $(CH_3NH_3)_4PbI_6{\cdot}2H_2O$ hydrates [153]. It has been established that water molecules are degradation catalysts. Degradation of organic-inorganic perovskites under the effect of moisture can occur due to the formation of $(CH_3NH_3PbI_3{\cdot}H_2O)$ monohydrate and $[(CH_3NH_3)_4PbI_6{\cdot}2H_2O]$ dihydrate. The formation of these phases occurs under conditions of fairly high moisture (usually >70-80%) [164]. The main products of perovskite degradation in environmental conditions can be $PbCO_3$, $Pb(OH)_2$, α-PbO, and β-PbO in addition to PbI_2 [155].

It should be noted that the layers around the perovskite in the cell also have a significant effect on stability. Thus, the use of a material, such as HTL, with hydrophobic properties will improve stability compared to spiro-OMeTAD and PTAA. In addition, the stability can be improved by using a hydrophobic layer coating of the cell itself. Hwang et al. obtained increased stability by a light hydrophobic passivation technique using a polytetrafluoroethylene coating, which provided a slight degradation after 30 days in the ambient atmosphere [146]. Degradation due to moisture can be significantly reduced by adding a thin blocking layer of Al_2O_3 between HTL and perovskite film [24]. Replacement of Pb by Sn leads to increased sensitivity of perovskite films to moisture. Therefore, lead-free perovskite-based cells require encapsulation. Glass and resin that hardens under the action of UV radiation are used for this purpose [149].

Perovskite film does not interact with oxygen in the absence of light [144, 156, 157]. Illumination leads to the excitation of electrons in the conduction band and the oxidation of molecular oxygen, forming $O_2^{\cdot-}$ superoxide. This further destroys the MA cation and forms CH_3NH_2, I_2, PbI_2, and water [158]. The formation of superoxide under light is the main cause of chemical degradation of organic-inorganic perovskite [159, 160].

In this regard, an important finding of the study [161] showed that the natural dye carotene is an effective dopant of the PSC film. It increases its PCE. At the same time, carotene is an effective suppressor of singlet oxygen and superoxide. Therefore, its introduction into the perovskite film can be another factor in improving its stability.

Thermal instability is another PSC problem. Solar cells must withstand elevated temperatures, as the operating temperature for solar cells is 40 to 85°C. $MAPbI_3$ has a low thermal conductivity [162] and also decomposes at 85°C even in an inert atmosphere [163]. The heat caused by irradiation is difficult to eliminate. Coining et al. reported that perovskites decompose, forming PbI_2 when heated under nitrogen at 85°C until complete removal of the organic component (MA). A stable photocell must be thermostable up to 85°C [164]. The energy range of $MAPbI_3$ formation is 0.11-0.14 eV. Decomposition of the perovskite film occurs at a temperature of 100-140°C [54].

The *ab initio* molecular dynamics states that the increase in vibration and rotation of the methylammonium group, which occurs at elevated temperatures, contributes to the decomposition of the stable lattice of $MAPbI_3$ to PbI_2 and volatile compounds [165]. However, $MAPbI_3$ will not decompose even at higher temperatures in the absence of defects in surfaces and grain boundaries. Thus, the combination of lattice defects and MA mobility is the cause of thermal instability of this compound. It is shown that the partial replacement of I by Br or Cl makes the lattice more flexible and tolerant to the mobility of the MA group, which stabilizes the Pb-halide lattice. An additional effect of increasing stabilization is preventing the formation of thermally stable PbI_2 grains, which act as crystallization nuclei. These findings were confirmed by X-ray photoelectron spectroscopy of specially prepared annealed $MAPbI_3$, $MAPbI_{2.7}Br_{0.3}$, $MAPbI_{2.7}Cl_{0.3}$, and $MAPbBr_3$ films [165].

A larger FA cation was used instead of MA to combat instability. It has been shown that a $MAPbI_3$ film is converted to PbI_2 at 60°C, whereas $FAPbI_3$ withstood this temperature for up to 60 min [166]. The replacement of the MA organic cation by FA increases the tolerance factor to 0.99, which improves thermal stability [87]. The thermal stability of the cells was also successfully increased by replacing organic HTL with single-walled carbon nanotubes [167]. The use of spiro-OMeTAD as HTL is also one of the causes of PSC thermal degradation. Arora et al. increased the PSC thermal stability by using copper(I) thiocyanate (CuSCN) as a hole transport layer. In this case, the cell withstood 1000 h of testing at 60°C in sunlight and successfully retained 95% of PCE [168].

The degradation of perovskite-based solar cells through lighting is an important factor in determining stability, as any solar cell is exposed to light and electrical displacement to generate electricity. TiO_2 is widely used as ETL in the PSC manufacture, but due to the size of its band gap of 3.2 eV and the presence of redox properties, it acts as a photocatalytic material. Snaith studied the degradation of perovskite-based solar cells by UV radiation and stated that a titanium oxide-based photoanode promotes the rapid PSC decomposition. Some researchers have suggested that doping the TiO_2 layer with Ga^{3+}, Nd^{3+}, and Al^{3+} trivalent cations can lead to a decrease in the number of oxygen vacancies [169, 170]. Wojciechowski et al. replaced the titanium oxide layer with fullerene (C_{60}), which increased the stability of the device [171]. When illuminated, the degradation products of perovskites are PbI_2, NH_3, CH_3I, CH_3NH_2, HI, and I_2 [172]. The study [173] reported that the crystal properties of coarse-grained PSC degrade under illumination due to the formation of metastable traps, which leads to inhomogeneity of the electric field in the perovskite and reduce photocurrent. Light-induced degradation of $MAPbI_3$ was studied under different conditions in the work [174]. There was no degradation in the N_2 atmosphere. However, perovskite degrades to metallic lead without illumination in vacuum, and to PbI_2 under illumination.

The quality of perovskite film is crucial for creating highly efficient and stable solar cells [175]. Such a film is usually made by solution deposition at low temperature and therefore contains polycrystals with a large number of defects, such as uncoordinated ions and free bonds on the surface along the grain boundaries, as well as inside the main grains [176, 177]. These defects can cause recombination of charge centers, which leads to energy loss and, consequently, reduce device performance [178, 179]. In addition, these defects are sensitive to light and heat (have low activation energy) and can initiate the penetration of moisture, which significantly reduces the stability of the device [180-183].

Chemical compounds capable of forming hydrogen or coordination bonds with perovskite molecules can passivate defects in its structure when used as additives [184, 185]. In addition, polymer molecules, due to their long chains, can crosslink the boundaries of perovskite grains, thus increasing mechanical stability and durability of perovskite-based solar cells [186]. The choice of additives includes small organic molecules [187-189], inorganic salts [190], long-chain polymers [191], ionic liquids [183], etc.

The study [175] describes the strategy of using organic dyes as additives that passivate defective states of perovskite. Dyes used for textile dyeing have been successfully used for this matter due to their high ability to form intermolecular hydrogen bonds, low cost, excellent photochemical properties, high ecological compatibility, charge mobility, and ease of chemical structure modification [192]. In addition, the optical band of organic dyes can promote additional light capture and

subsequent energy transfer to perovskite films [193, 194]. Therefore, such dyes are promising PSC additives. In particular, the simple and cost-effective 5-chloroisatin organic dye (isatin-Cl) as an additive to the $CH_3NH_3PbI_3$ film not only effectively passivates defects but also stimulates the growth of *n*-type film density. The result is an increase in PCE of the modified isatin-Cl perovskites from 18.13% to 20.18% with a significant improvement in V_{oc}, J_{sc}, and FF, as well as a slight hysteresis compared to the control samples [175]. In addition, the fixation of hydrophobic isatin-Cl between the grains and on the upper surface of the film by hydrogen bonds that form CO and NH isatin-Cl with hydrogen and halogen atoms of perovskite significantly increases the stability of solar cells against moisture and temperature fluctuations. The passivated PSC shows a drop in PCE of only 10% after 350 h at 45% relative humidity, while the efficiency of the initial device decreases by 45% over the same time. The results of the study [175] show a new strategy using cheap and non-toxic organic dyes as additives in the formation of perovskite films to increase the efficiency and environmental stability of solar cells based on them.

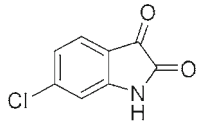

Isatin-Cl

The presence of harmful traps in the perovskite film due to uncoordinated Pb^{2+} ions can be minimized with the help of organic dyes with carboxyl groups. Thus, the use of AQ310 dye in the study [195] increased the PCE from 17.98% to 19.43%. It should be noted that the covalently bound COOH group of the donor-acceptor polyene plays a positive role, as it promotes charge separation in the PSC.

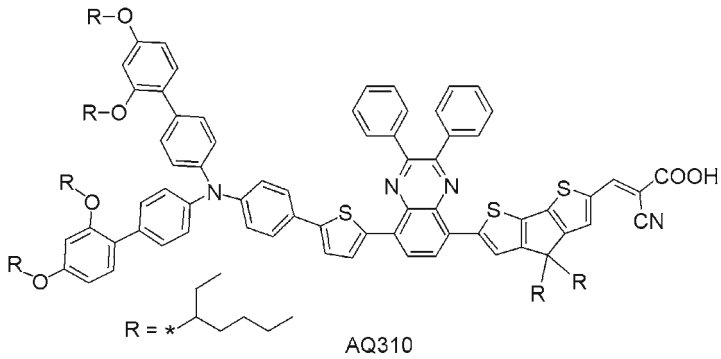

AQ310

It is significant that the replacement of the ester group in the PCBM molecule with a carboxyl one (PCBA) enhances the adhesion to the metal oxide surface to such an extent that the latter compound must be deposited 100 times less than the former with the same efficiency and stability of PSC. Such a significant reduction in the expensive fullerene derivative points the way for the development of new hybrid transport materials for upscaled PSC with improved efficiency and stability.

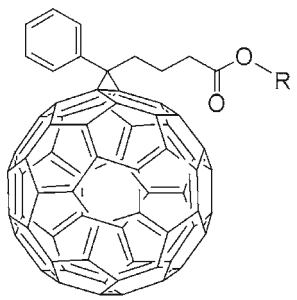

PCBM, R = Me
PCBA, R = H

The study [197] suggested using organic luminophores for protection against UV radiation, which work on the principle of re-emission of light energy from the high-energy spectral range to the low-energy one. In this case the effective luminophores must have [198]:

– high value of extinction in the UV region of the spectrum for efficient capture of photons in this region;

– large Stokes shifts to convert high-energy destructive UV radiation into light with less energy in the visible spectral range. In this case, the Stokes shift should reach such a value that the maximum radiation of the luminophore falls in the region of high intensity of the absorption band of perovskite, ensuring the maximum transfer of excitation energy from the luminophore to perovskite. A significant Stokes shift is also required to minimize fluorescence attenuation by reducing the reabsorption phenomenon caused by the overlap of the organic luminophore radiation bands and the perovskite absorption band;

– high fluorescence quantum yield for high-quality conversion of re-radiation energy;

– low tendency to aggregation, as it is accompanied by fluorescence attenuation [199], and in some cases even a decrease in the photostability of the luminophore [200].

The commercial Lumogen F Violet 570 compound (V570) was chosen as a luminophore in the study [197].

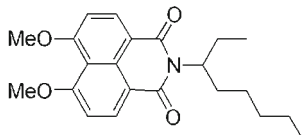

V570

Analysis of its chemical structure showed that the high fluorescence quantum yield is due to the structural rigidity and planarity of the chromophore [201]. The large Stokes shift is the result of a strong change in the electron density during excitation because the boundary structures of ground and excited states are very different in intraionic compounds: the former is electroneutral, and the latter is dipolar. The low tendency to aggregation is associated with the dominance of the neutral boundary structure in the ground state, which minimizes the association of monomer molecules due to electrostatic gravitation [203].

Currently, there are many different effective inorganic and organic UV absorbers that can potentially be used to protect organic-inorganic perovskites. Recently, CsBr has been widely used for this purpose as an interphase modifier between perovskite layers, but its resistance to moisture and high temperatures is unsatisfactory [204]. In addition, it acts only as a subtractive light filter, capable only of cutting off UV radiation without converting it into visible light. This disadvantage is typical for many other organic absorbers [205]. The ability of V570 luminophores to convert harmful UV radiation into useful visible radiation not only provides reliable protection from the sun's ultraviolet light and artificial sources, but also allows one to further increase the PCE, in this case up to 6%. The luminescent solar concentrators use this working principle and are used to increase the current capacity of silicon photoelectric converters of solar energy into electricity [206].

The authors of the study [197] successfully used a photopolymer based on chlorotrifluoroethylene vinyl ether and dimethacrylic perfluoropolyether oligomer with high hydrophobicity to provide protection against moisture. It is quite transparent in the field of light absorption by V570 luminophore, chemically inert to it, and dissolves it well. Therefore, it was possible to create a polymer film coated with V570 luminophore, which provided protection against both moisture and UV radiation. It is worth noting that its deposition gave significant positive results not only in the laboratory but also in real atmospheric conditions, where the temperature changed and heavy rainfall occurred during the month. During this period the efficiency of solar cells was 95% of the original one under such conditions [197].

One of the problems of the fluorinated polymer proposed in the study [197] may be the photopolymerization of its production. It is known that both photoinitiation and free radical reaction in many cases can cause the destruction of not only organic luminophore, but also the components of the photoactive layer [200]. Therefore, it is desirable to use less aggressive polymerization methods, such as polycondensation [207]. Ready-made polymers can be used in many cases [71, 208, 209]. Thus, this study showed that the coating of perovskite with a polyvinyl butyral film also increases its stability to atmospheric conditions [71].

There are other factors that affect the stability and efficiency of the PSC device, apart from moisture, oxygen, temperature, and lighting. These include the use of certain additives in different layers, which affects the selectivity of the contacts and the transition supports of the interfaces (ETL/perovskite and HTL/perovskite). Manufacturing technology and electrical displacement also have an important influence [149].

The exact correspondence of the energy levels of the limit orbitals of dopant and perovskite is crucial when choosing impurity molecules for ETL and HTL layers. According to the above-mentioned data, promising materials for the hole transport are theoretically predicted and synthesized fluorescently substituted analogues of spiro-OMeTAD compound [210] and star-like substituted phenols in *ortho* and *para* positions by aromatic electron donors [211], which allow one to ensure high efficiency and thermostability of photovoltaic cells. In particular, a certified efficiency of 22.6% was reached, and 95% of the initial productivity was retained for more than 500 h after thermal annealing at 60°C when using the first one.

According to theoretical modeling by density functional theory (DFT) and molecular dynamics, it is proposed to use NP4 carbazole-substituted N-annelated perylene as a hole transport material for the perovskite film [212].

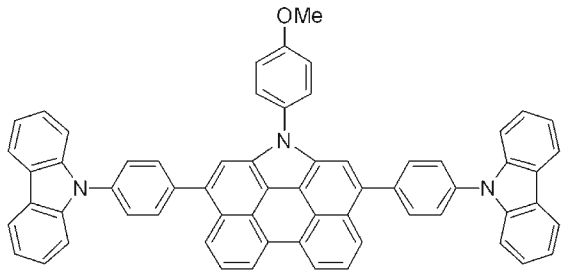

NP4

The possible advantages of the carbazole substituent are highlighted in comparison with the triphenylamine derivatives, which is currently the most popular group, due to its powerful electron donor ability. It is shown that the NP4 compound has a deeper level of HOMO energy, which is advantageous for achieving higher V_{oc} and shorter lifetime of the excited state, which reduces the negative effect of its relaxation. It also has a lower energy of electron–hole separation, greater mobility of holes due to the ideal "face to face" configuration, and the shortest distance between the centers of molecules. The electronic and optical properties of the carbazole structure are more easily modified by other functional groups [212].

The difference between the HOMO energy levels of the NP4 compound and the valence band of perovskite increases further in the adsorbed NP4-$CH_3NH_3PbI_3$ system, which increases the driving force of the hole exit [212].

The study [213] showed the multifunctionality of additives of small organic molecules in perovskite films in the process of their production. Thus, the DBP molecule, on the one hand, equalizes the energy levels of the interface between the perovskite layer and ETL, thereby reducing losses due to recombination of charge carriers. On the other hand, a strongly luminescent DBP increases the efficiency of light absorption by the active layer of $CH_3NH_3PbI_3$ in the near IR range of the spectrum by transferring energy from the DBP to perovskite using Forster resonance energy transfer. The result of these effects is a significant improvement in the PCE of the solar perovskite cell. In addition, the hydrophobic DBP molecule, by passivating defects in the structure of the perovskite film, blocks its erosion due to temperature, ion/molecule diffusion, moisture, and oxygen [213].

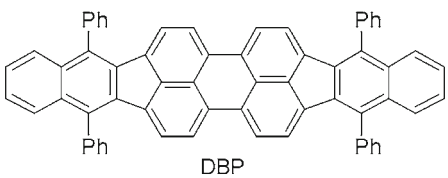

DBP

A new organic IEICO-4F semiconductor has been synthesized, which combines a Lewis base and a deep-dyed chromophore. The former determines its ability to coordinate with perovskite, which in turn passivates defects in the structure of the film of the latter, reducing the concentration of traps and ion migration caused by light and increasing the mobility of

holes and electrons. The intense absorption of light by the dye in the region above 800 nm increases the photocurrent generation and the photoelectric efficiency of the PSC in the near-IR range, where perovskite does not operate. As a result, perovskite solar cells with IEICO-4F dye show an increased efficiency of 21.6% and significantly improve the operational stability under constant sunlight [214].

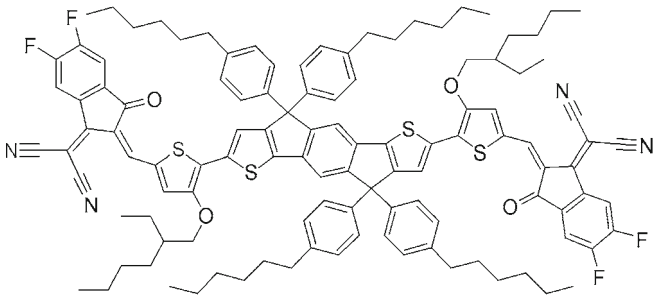

IEICO-4F

The study [215] showed an increased PSC efficiency due to cationic polyelectrolytes based on unconjugated polyethyleneimine salts with different anions: bromide, iodide, and tetraimidazolylborate. A dipole occurs between the salt and metal electrode when this salt is introduced into the ETL. It is possible to control the electronic level energy and the electronic work function by changing the nature of the anion. The magnitude of the effect naturally increases when the anion size is increased by using bromide, iodide, and tetraimidazolylborate [215].

A perovskite and DSSC-based tandem solar device was created. The latter is TiO_2 powder, which adsorbed dichromophore dye from the solution. The photoelectric properties of the device increased compared to individual PSC and DSSC. However, the photocurrent was low because it was limited by the J_{sc} value of the lower DSSC in tandem configuration [216].

One of the problems that affect the stability of organic-inorganic perovskite-based solar cells is the presence of ion migration. A deep understanding of the mechanisms of ion migration is important in the development of organic-inorganic perovskites-based devices, which would increase their stability. This problem drew much attention after the detection of photocurrent hysteresis in solar cells [217-220]. The authors of [221] proposed to consider the mechanism of ion migration to explain the photocurrent hysteresis phenomenon in the perovskite-based solar cell. The authors study the results of ion migration in organic-inorganic perovskites [222]. Many experimental data confirm the migration of ions in organic-inorganic perovskites. However, additional data are needed to understand the effect of ion migration on the properties of solar cells and how to prevent their unwanted effects.

It should be noted that ion migration in perovskite significantly reduces the PSC properties and leads to the hysteresis of the volt-ampere characteristics (VAC) of the cell [223, 224]. It should also be noted that, unlike perovskites, there are no problems associated with ion migration in light-sensitive materials such as silicon. The causes of ion migration in perovskite may include processes at grain boundaries, in particular the presence of moisture, since hysteresis was not observed in studies of single crystals [225] as well as polycrystals in a dry atmosphere [226]. The study of *J-V* dependences in a single crystal of organic-inorganic perovskites was performed by the authors of [225]. $MAPbI_3$ single crystals were synthesized by the antisolvent method, and the study of *J-V* dependences wA performed by the four-probe method [225]. Two types of contacts were used: one that injects electrons (contact with Ti) and the other that injects holes (contact with MoO_3/Au/Ag). In both cases, the authors observed three areas in the VAC: the VAC are described by Ohm's law at low voltages and by Child's law ($J \sim V^2$) at increasing voltages; in addition, a transition region was present.

It should be noted that it is necessary to prevent changes in the microstructure and properties of the samples over time and under the action of moisture during the experiment when studying such characteristics of the samples in polycrystalline systems [227]. Therefore, in [226], studies using a dry atmosphere were conducted, and the films were deposited on a glass supporter using gold electrodes to measure the *J-V* dependences of freshly prepared polycrystalline films (Fig. 6).

The calculation of the film parameters (dielectric constant and current density) was performed using *J-V* partial capacitance method [228]. According to this approach, the measured multilayer system was represented as three simple planar capacitors with a homogeneous filling that were connected in a parallel way. The capacity of the multilayer system was

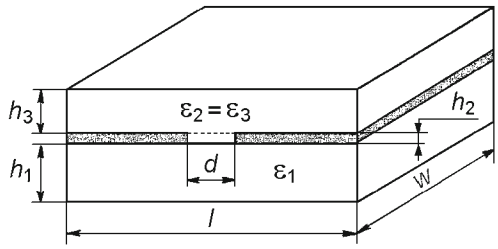

Fig. 6. Scheme of the measured multilayer system consisting of a substrate (l = 16 mm, w = 24 mm, h_1 = 1 mm), on which electrodes with a thickness of h_2 = 90 nm at a distance d = 250 μm and the studied film with a thickness of h_3 = 500 nm were deposited. Submitted according to the study data [226] with the permission of SpringerOpen under Creative Commons Attribution 4.0 International License http://creativecommons.org/licenses/by/4.0/.

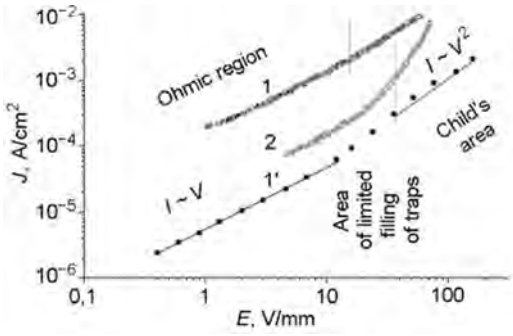

Fig. 7. Dependence of the current density on the intensity of organic-inorganic perovskite at room temperature (295 K) in the form of a single crystal (*1*) and a polycrystalline film (*1′*), as well as a single crystal at a temperature of 250 K (*2*). Prepared according to the study data [225, 226] with the permission of SpringerOpen under Creative Commons Attribution 4.0 International License http://creativecommons.org/licenses/by/4.0/.

determined as the sum of the capacities of the substrate, the inner rectangular part of the film, and the outer rectangular part of the film (Fig. 6). The substrate capacity and the capacity of the outer part of the film were determined using conformal mappings based on the Schwarz-Christoffel transformation, adapted in Gevorgyan's approach [229]. The experimentally determined dielectric constant of the film in the frequency range of 1 Hz - 1 MHz was ε = 52; this value is consistent with the published data [230].

The *J-V* dependences obtained for single crystal [225] and polycrystal [226] studied in a dry atmosphere are similar to each other (Fig. 7, curves 1 and 1′), which indicates the decisive influence of the grain boundary processes on hysteresis. The transition from Ohm's law to Child's law is observed more clearly when the temperature of the study decreases (Fig. 7, curve 2).

Grancini et al. created a 2D/3D structure of $(HOOC(CH_2)_4NH_3)_2PbI_4/CH_3NH_3PbI_3$ and prepared PSC based on it using carbon electrodes. The cell efficiency was 12.9%. The 10×10 cm size solar cells with a high efficiency of 11.2% were made using printing technology. The cells showed stable performance for more than 400 days with an extremely small decrease in efficiency over time [231].

Another problem with $CH_3NH_3PbI_3$-based solar cells is the toxicity of the components used in the development. $CH_3NH_3PbI_3$-based organic-inorganic perovskite contains lead. Lead toxicity can pose serious health risks. Lead is partially replaced by other low-toxicity metals, or lead is completely eliminated using other metals, such as Sn^{2+}, Sn^{4+}, Ge^{2+}, Cu^{2+}, Bi^{3+}, and Sb^{3+}, to avoid problems with the presence of lead in perovskite [232]. Unfortunately, Sn-based PSCs have not been widely used. Cells show stable but low PCE in the development of Sn^{4+}-based PSC, while the use of perovskites, which include Sn^{2+}, leads to low stability of PSC [233].

A new component must demonstrate a high level of PSC performance and high stability, must be compatible with large-scale manufacturing technologies, and must have a low cost to replace Pb in PSC.

It should be noted that PSC is not the only solar cell that contains toxic materials. There are other toxic materials in traditional solar cells, which are widely used in practice, such as indium cuprate, cadmium telluride, indium gallium cuprate (di-)selenide, cadmium gallium (di-)selenide, hexafluoroethane, and polyvinyl fluoride. Silicon tetrachloride, which is a by-product in the production of crystalline silicon, is also very toxic. Moreover, the amount of lead used in the PSC is very small compared to the lead used in other common devices, such as lead-cadmium batteries, integrated circuits, infrared detectors, etc. The amount of lead does not exceed 0.4 g/m^2 in the case of $CH_3NH_3PbI_3$ perovskite-based solar cells, which is less compared to the lead used in commercial Si-based PV-panel soldering [233]. Nowadays, lead-free PSC show significantly lower efficiency. Therefore, the main focus should be on increasing stability in the development of perovskite-based PSC.

CONCLUSIONS AND PROSPECTS

There has been a revolution in the area of research during the last 10 years since the discovery of the ability of organic-inorganic perovskites to convert solar energy into electricity [234]. The World Economic Forum recognized perovskite-based solar cells as one of the 10 most significant technologies in 2016. [235]. Organic-inorganic perovskites are characterized by a set of important photo- and electrophysical properties. They are easy to obtain from common metal salts and industrial chemical organic compounds, rather than from expensive and rare elements used in highly efficient silicon and gallium arsenide-based semiconductor analogues.

A significant advantage of perovskite technology in the manufacture of solar cells compared to traditional silicon one is that the active PSC layers can be deposited from liquid solutions on thin and flexible supporters. This allows one to place solar panels on surfaces of any curvature and to develop a variety of designs: window translucent “energy curtains” for houses and cars, facades and roofs, consumer electronics, gadgets, etc.

It is necessary to ensure high performance, stable operation, and low cost of PSC in order for perovskite-based solar cells to find wide practical application. Today, the best laboratory samples of PSC demonstrate high efficiency (which is not inferior to silicon-based solar cells) and low production costs. However, they have relatively low stability, although some PSC show stable performance throughout the year [24, 236].

As a rule, small PSC (0.03-0.2 cm^2) have high efficiency but are not suitable for practical application. Therefore, it is important to manufacture large area devices (1 cm^2 or more) while maintaining the same efficiency as in the case of small area devices and reliable stability [237]. Oxford PV company reported the development of a perovskite-silicon tandem cell (1 cm^2), which reached the highest PCE value of 28% [238]. Toshiba, New Energy, and Industrial Technology Development Organization (NEDO) have developed a large-size module of 703 cm^2 (24.15×29.10 cm), which solves the problem of large perovskite-based solar cells, which demonstrate relatively high efficiency [239]. Saule Technologies has installed a PSC module in an innovative Japanese hotel called Henna. The installed commercial prototype includes 72 PSC modules [240]. These results indicate significant progress in the development of organic-inorganic perovskites and solar cells based on them, which has been achieved in a relatively short period of time and gives hope for their widespread commercialization in the future.

The quality of perovskite film is crucial for creating highly efficient and stable solar cells. Typically, such films are obtained by precipitation from solutions and contain a significant number of defects. The phase transformations that occur when the ratio of starting reagents and solvents changes are studied to determine the nature of the film stability. Chemical compounds capable of forming hydrogen or coordination bonds with perovskite molecules are used, which allows one to passivate the existing defects and crosslink the boundaries of perovskite grains and, as a result, improve mechanical stability and increase the PSC durability. In particular, organic dyes as additives can passivate the defective state of perovskite. For example, harmful traps in the perovskite film caused by uncoordinated Pb^{2+} ions can be neutralized by organic dyes with carboxyl groups [195, 196].

The problem of instability of perovskite-based solar cells remains relevant. It depends on both the quality of perovskite films and on the components of solar cells, primarily HTL and ETL. Therefore, it is important to study their effect on the PSC stability. In particular, thermal stability can be increased by replacing spiro-OMeTAG as a hole conductor with copper(I) thiocyanate (CuSCN), as well as by partial replacement of iodine with chlorine and bromine in perovskite [165]. The stability of organic-inorganic perovskite-based solar cells can be increased by improving the properties of the electron transport layer (ETL), where TiO_2 is often used by doping with trivalent cations (Ga^{3+}, Nd^{3+}, Al^{3+}), which can reduce the number of oxygen vacancies, thereby reducing the degradation of perovskite under light. Replacing the TiO_2 layer with fullerene (C_{60}) also increases stability.

New opportunities arise when combining perovskites with unique light energy converters, such as organic dyes [122, 127]. An important aspect in the development of this field is that the crystal structure of the former, despite the high tolerance factor, can withstand mixing in one layer with the latter [122]. It also makes it possible to combine the best properties of perovskite and dye in one material, which was done in the study [122]. Only the first steps have been taken in this application of dyes. Their enormous potential is hardly revealed. In particular, one can expect extraordinary effects from the use of zwitterionic [133, 241] and merocyanine dyes [242]. Their potential includes the following facts: the absence of a counterion excludes ionic conductivity, which is especially harmful for photovoltaics [243]; strong intra-molecular redistribution of electron density upon excitation enables photogeneration of both holes and electrons in one molecule [244]; the possibility of decreasing or increasing the dipole moment depending on the chemical structure during the transition to the electronically excited state determines diametrically opposite applications [242]; in contrast to ionic dyes, they can be sublimated even at high temperatures [245], which allows them to be deposited directly on photoconductive supporters without solvent by gas spraying [246].

Another source of organic dyes is J-aggregates [247] as a variety of highly ordered nanostructures [247-251]. They are characterized by extremely weak vibronic interactions. The consequence of this is a record intensity and narrowness of the absorption bands [247-251], as well as the propagation of exciton excitations with minimal losses in the J-aggregate chains [248]. The last factor should be particularly attractive in terms of the impact on the transport of charge carriers in perovskite when mixed with a dye [122, 248]. Plasmonic metal nanoparticles can have an additional effect on both the former and the latter because the oscillations of the conduction electrons considerably amplify the local electromagnetic field of the crystal lattice of the metal when excited by light, which significantly enhances optical processes in molecules and clusters [252, 255]. Such effects have already been observed in organic dyes [254, 255] and perovskites [256]. Therefore, the implementation of these effects in their hybrid composition is of considerable scientific and practical interest.

PSC toxicity is definitely an important issue. It is desirable to replace lead in organic-inorganic perovskites. Unfortunately, the known lead-free perovskites show a lower level of properties. The development of lead-free organic-inorganic perovskites is an important task. However, according to the authors, the most important problem at this stage is to increase the stability of solar cells.

This study was performed with the financial support of the target program of the fundamental research of the National Academy of Sciences of Ukraine "Prospective fundamental research and innovative development of nanomaterials and nanotechnologies for industry, healthcare, and agriculture," project No. 0120U102242.

REFERENCES

1. D. M. Chapin, C. S. Fuller, and G. L. Pearson, *J. Appl. Phys.,* **25,** 676-677 (1954), doi: 10.1063/1.1721711.

2. A. G. Martin, E. Keith, H. Yoshihiro, et al., *Prog. Photovoltaics*, **20,** 12-20 (2012), doi: 10.1002/pip.2978.
3. B. O'Regan and M. Grätzel, *Nature*, **353,** 737-740 (1991), doi: 10.1038/353737a0.
4. K. Okadzaki, *Ceramic Dielectric Technology* [in Russian], Energiya, Moscow (1976).
5. A. N. Suslov, D. A. Durilin, O. V. Ovchar, et al., *Inorg. Mater.*, **50,** 1125-1130 (2014), doi: 10.1134/S0020168514110193.
6. V. Jella, S. Ippili, J.-H. Eom, et al., *Nano Energy*, **57,** 74-93 (2019), doi: 10.1016/j.nanoen.2018.12.038.
7. A. G. Belous, O. Z. Yanchevskii, O. I. V'yunov, et al., *Inorg. Mater*., **44,** 414-419 (2008), doi: 10.1134/S002016850804016X.
8. J. M. Tarascon, L. H. Greene, P. Barboux, et al., *Phys. Rev. B*, **36,** 8393 (1987), doi: 10.1103/PhysRevB.36.8393.
9. O. Z. Yanchevskii, A. I. Tovstolytkin, O. I. V'yunov, et al., *Inorg. Mater*., **44,** 181-188 (2008), doi: 10.1134/S0020168508020180.
10. A. G. Belous, O. I. V'yunov, O. Z. Yanchevskii, et al., *Inorg. Mater*., **42,** 286-293 (2006), doi: 10.1134/S0020168506030149.
11. A. G. Belous and S. D. Kobylyanskaya, *Oxide-Based Lithium Conductive Solid Electrolytes* [in Russian], Naukova Dumka, Kiev (2018).
12. A. G. Belous, *High-Quality Ultra-High-Frequency Dielectrics* [in Russian], Naukova Dumka, Kiev (2016).
13. A. G. Belous and O. I. Vyunov, *Ukr. Khim, Zh*., **78,** 3-31 (2012), doi: 10.5281/ZENODO.3822595.
14. Y. Zhao and K. Zhu, *Chem. Soc. Rev*., **45,** 655-689 (2016), doi: 10.1039/C4CS00458B.
15. D. Weber, *Z. Naturforsch*, **33b,** 862-865 (1978).
16. D. Weber, *Z. Naturforsch*, **33b,** 1443-1445 (1978).
17. W. -J. Yin, J. -H. Yang, J. Kang, et al., *J. Mater. Chem. A*., **3,** 8926-8942 (2015), doi: 10.1039/C4TA05033A.
18. Z. Fan, K. Sun, and J. Wang, *J. Mater. Chem. A*, **3,** 18809-18828 (2015), doi: 10.1039/C5TA04235F.
19. A. Kojima, K. Teshima, Y. Shirai, et al., *J. Am. Chem. Soc*., **131,** 6050-6051 (2009), doi: 10.1021/ja809598r.
20. H.-S. Kim, C.-R. Lee, J.-H. Im, et al., *Sci. Rep*., **2,** 591 (2012), doi: 10.1038/srep00591.
21. M. M. Lee, J. Teuscher, T. Miyasaka, et al., *Science*, **338,** 643-647 (2012), doi: 10.1126/science.1228604.
22. J. H. Heo, S. H. Im, J. H. Noh, et al*., Nat. Photonics*, **7,** 486 (2013), doi: 10.1038/nphoton.2013.80.
23. Best Research-Cell Efficiency Chart, (2020). (accessed 15 May, 2020).
24. A. Mei, X. Li, L. Liu, et al., *Science*, **345,** 295-298 (2014), doi: 10.1126/science:1254763.
25. D. A. Valverde-Chavez, C. S. Ponseca, C. C. Stoumpos, et al., *Energy Environ. Sci*., **8,** 3700-3707 (2015), doi: 10.1039/c5ee02503f.
26. A. Miyata, A. Mitioglu, P. Plochocka, et al., *Nature Phys*., **11,** 582-587 (2015), doi: 10.1038/nphys3357.
27. G. Xing, N. Mathews, S. Sun, et al., *Science,* **342,** 344-347 (2013), doi: 10.1126/science:1243167.
28. V. Gonzalez-Pedro, E. J. Juarez-Perez, W.-S. Arsyad, et al., *Nano Lett*., **14,** 888-893 (2014), doi: 10.1021/nl404252e.
29. Y. Zhao and K. Zhu, *Chem. Soc. Rev*., **45,** 655-689 (2016), doi: 10.1039/C4CS00458B.
30. M. B. Johnston and L. M. Herz, *Acc. Chem. Res*., **49,** 146-154 (2016), doi: 10.1021/acs.accounts.5b00411.
31. H. Tang, S. He, and C. Peng, *Nanoscale Res. Lett*., **12,** 410 (2017), doi: 10.1186/s11671-017-2187-5.
32. P. Roy, N. K. Sinha, S. Tiwari, et al., *Sol. Energy*, **198,** 665-688 (2020), doi: 10.1016/j.solener.2020.01.080.
33. H.-S. Kim, S. H. Im, and N.-G. Park, *J. Phys. Chem. C*, **118,** 5615-5625 (2014), doi: 10.1021/jp409025w.
34. G. Giorgi and K. Yamashita, *J. Mater. Chem. A*, **3,** 8981-8991 (2015), doi: 10.1039/C4TA05046K.
35. G. A. Smolenskiy, V. A. Bokov, V. A. Isupov, et al., *Ferroelectrics and Anti-ferroelectrics* [in Russian], Nauka, Leningrad (1971).
36. V. M. Goldschmidt, T. Barth, G. Lunde, et al., *I. Mat.-Naturv. KI*, **2,** 117 (1926).
37. G. A. Smolensky and A. I. Agranovskaya, *Zh. Tekh. Fiz*., **28,** 1491-1493 (1958).
38. A. Poglitsch and D. Weber, *J. Chem. Phys*., **87,** 6373-6378 (1987), doi: 10.1063/1.453467.
39. N. Onoda-Yamamuro, T. Matsuo, and H. Suga, *J. Phys. Chem. Solids,* **51,** 1383-1395 (1990), doi: 10.1016/0022-3697(90)90021-7.
40. Y. Kawamura, H. Mashiyama, and K. Hasebe, *J. Phys. Soc. Jpn.*, **71,** 1694-1697 (2002), doi: 10.1143/jpsj.71.1694.
41. A. F. Kapustinskii and K. B. Yatsimirskii, *Zh. Obshch. Khim*., **19,** 2191-2200 (1949).
42. G. Kieslich, S. Sun, and A. K. Cheetham, *Chem. Sci*., **5,** 4712-4715 (2014), doi: 10.1039/C4SC02211D.

43. A. Dualeh, N. Tetreault, T. Moehl, et al., *Adv. Funct. Mater*., **24,** 3250-3258 (2014), doi: 10.1002/adftn.201304022.
44. Y. Zhao and K. Zhu, *J. Phys. Chem. Lett*., **4,** 2880-2884 (2013), doi: 10.1021/jz401527q.
45. Y. Zhao, A. M. Nardes, and K. Zhu, *J. Phys. Chem. Lett.*, **5,** 490-494 (2014), doi: 10.1021/jz500003v.
46. Y. Wu, A. Islam, X. Yang, et al., *Energy Environ. Sci.,* **7,** 2934-2938 (2014), doi: 10.1039/C4EE01624F.
47. N. J. Jeon, J. H. Noh, W. S. Yang, et al., *Nature*, **517,** 476-480 (2015), doi: 10.1038/nature14133.
48. S. Ryu, J. Seo, S. S. Shin, et al., *J. Mater. Chem. A*, **3,** 3271-3275 (2015), doi: 10.1039/C5TA00011D.
49. N. J. Jeon, H. G. Lee, Y. C. Kim, et al*., J. Am. Chem. Soc.,* **136,** 7837-7840 (2014), doi: 10.1021/ja502824c.
50. J. Seo, S. Park, Y. C. Kim, et al., *Energy Environ. Sci*., **7,** 2642-2646 (2014), doi: 10.1039/C4EE01216J.
51. G. E. Eperon, V. M. Burlakov, P. Docampo, et al., *Adv. Funct. Mater.*, **24,** 151-157 (2014), doi: 10.1002/adfm.201302090.
52. H. Zhou, Q. Chen, G. Li, et al., *Science*, **345,** 542-546 (2014), doi: 10.1126/science.1254050.
53. J. You, Y. Yang, Z. Hong, et al., *Appl. Phys. Lett*., **105,** 183902 (2014), doi: 10.1063/1.4901510.
54. B. Philippe, B.-W. Park, R. Lindblad, et al., *Chem. Mater*., **27,** 1720-1731 (2015), doi: 10.1021/acs.chemmater.5b00348.
55. C.-Y. Chang, C.-Y. Chu, Y.-C. Huang, et al., *ACS Appl. Mater. Interfaces,* **7,** 4955-4961 (2015), doi: 10.1021/acsami.5b00052.
56. Z. Wu, S. Bai, J. Xiang, et al., *Nanoscale*, **6,** 10505-10510 (2014), doi: 10.1039/C4NR03181D.
57. M. Saliba, K. W. Tan, H. Sai, et al., *J. Phys. Chem. C*, **118,** 17171-17177 (2014), doi: 10.1021/jp500717w.
58. K. Odysseas Kosmatos, L. Theofylaktos, E. Giannakaki, et al., *Energy Environ. Mater*., **2,** 79-92 (2019), doi: 10.1002/eem2.12040.
59. Y. Rong, X. Hou, Y. Hu, et al., *Nat. Commun*., **8,** 1-8 (2017), doi: 10.1038/ncomms14555.
60. N. De Marco, H. Zhou, Q. Chen, et al., *Nano Lett*., **16,** 1009-1016 (2016), doi: 10.1021/acs.nanolett.5b04060.
61. Q. Han, Y. Bai, J. Liu, et al., *Energy Environ. Sci*., **10,** 2365-2371 (2017), doi: 10.1039/C7EE02272G.
62. H. Dong, Z. Wu, J. Xi, et al., *Adv. Funct. Mater*., **28,** 1704836 (2017), doi: 10.1002/adfm.201704836.
63. Y. Xia, C. Ran, Y. Chen, et al., *J. Mater. Chem. A*, **5,** 3193-3202 (2017), doi: 10.1039/C6TA09554B.
64. P. W. Liang, C. Y. Liao, C. C. Chueh, et al., *Adv. Mater*., **26**, 3748-3754 (2014), doi: 10.1002/adma.201400231.
65. C.-C. Chueh, C.-Y. Liao, F. Zuo, et al., *J. Mater. Chem. A*, **3,** 9058-9062 (2015), doi: 10.1039/C4TA05012F.
66. W. Zhang, M. Saliba, D. T. Moore, et al., *Nat. Commun*., **6,** 1-10 (2015), doi: 10.1038/ncomms7142.
67. F. K. Aldibaja, L. Badia, E. Mas-Marza, et al., *J. Mater. Chem. A*, **3,** 9194-9200 (2015), doi: 10.1039/C4TA06198E.
68. D. Forgacs, M. Sessolo, and H. J. Bolink, *J. Mater. Chem. A,* **3,** 14121-14125 (2015), doi: 10.1039/C5TA03169A.
69. D. T. Moore, H. Sai, K. W. Tan, et al., *J. Am. Chem. Soc*., **137,** 2350-2358 (2015), doi: 10.1021/ja512117e.
70. Y. Wu, F. Xie, H. Chen, et al., *Adv. Mater*., **29,** 1701073 (2017), doi: 10.1002/adma.201701073.
71. P. V. Torchynyuk, O. I. V'yunov, A. A. Ishchenko, et al*., Ukr. Khim. Zh*., **85,** 31-43 (2019), doi: 10.33609/0041-6045.85.9.2019.31-41.
72. A. A. Petrov, I. P. Sokolova, N. A. Belich, et al., *J. Phys. Chem. C*, **121,** 20739-20743 (2017), doi: 10.1021/acs.jpcc.7b08468.
73. P. Torchyniuk, O. V'yunov, A. Ishchenko, et al., *Solid State Sci*., submitted (2020).
74. M. Xiao, F. Huang, W. Huang, et al., *Angew. Chem. Int. Ed.*, **53,** 9898-9903 (2014), doi: 10.1002/anie.201405334.
75. E. Della Gaspera, Y. Peng, Q. Hou, et al., *Nano Energy*, **13,** 249-257 (2015), doi: 10.1016/j.nanoen.2015.02.028.
76. A. G. Belous, O. I. V'yunov, S. D. Kobylianska, et al., *Russ. J. Gen. Chem*., **88,** 114-119 (2018), doi: 10.1134/S1070363218010188.
77. A. Belous, S. Kobylianska, O. V'yunov, et al., *Nanoscale Res. Lett*., **14,** 1-9 (2019), doi: 10.1186/s11671-018-2841-6.
78. K. Liang, D. B. Mitzi, and M. T. Prikas, *Chem. Mater*., **10,** 403-411 (1998), doi: 10.1021/cm970568f.
79. J. Burschka, N. Pellet, S.-J. Moon, et al., *Nature*, **499,** 316-319 (2013), doi: 10.1038/nature12340.
80. J. Qiu, Y. Qiu, K. Yan, et al., *Nanoscale*, **5,** 3245-3248 (2013), doi: 10.1039/C3NR00218G.
81. Q. Chen, H. Zhou, Z. Hong, et al., *J. Am. Chem. Soc*., **136,** 622-625 (2014), doi: 10.1021/ja411509g.
82. Z. Wei, H. Chen, K. Yan, et al., *Angew. Chem. Int. Ed*., **53,** 13239-13243 (2014), doi: 10.1002/anie.201408638.
83. Y. Zhao and K. Zhu, *J. Mater. Chem. A*, **3,** 9086-9091 (2015), doi: 10.1039/C4TA05384B.
84. W. S. Yang, J. H. Noh, N. J. Jeon, et al., *Science*, **348,** 1234-1237 (2015), doi: 10.1126/science.aaa9272.

85. L. Su, Y. Xiao, L. Lu, et al., *Org. Electron.*, **77,** 105519 (2020), doi: 10.1016/j.orgel.2019.105519.
86. N. Ahn, K. Kwak, M. S. Jang, et al., *Nat. Commun*., **7,** 1-9 (2016), doi: 10.1038/ncomms13422.
87. H. J. Snaith, *J. Phys. Chem. Lett*., **4,** 3623-3630 (2013), doi: 10.1021/jz4020162.
88. N. Ahn, D.-Y. Son, I.-H. Jang, et al., *J. Am. Chem. Soc*., **137,** 8696-8699 (2015), doi: 10.1021/jacs.5b04930.
89. M. Liu, M. B. Johnston, and H. J. Snaith, *Nature,* **501,** 395-398 (2013), doi: 10.1038/nature12509.
90. Y. Liang, Y. Yao, X. Zhang, et al., *AIP Adv.,* **6,** 015001 (2016), doi: 10.1063/1.4939621.
91. S. Kavadiya, D. M. Niedzwiedzki, S. Huang, et al., *Adv. Energy Mater*., **7,** 1700210 (2017), doi: 10.1002/aenm.201700210.
92. A. Ummadisingu, L. Steier, J.-Y. Seo, et al., *Nature,* **545,** 208-212 (2017), doi: 10.1038/nature22072.
93. S. Kondo, H. Ohsawa, H. Asada, et al., *J. Appl. Phys*., **107,** 103526 (2010), doi: 10.1063/1.3374574.
94. V. M. Sorokin, N. V. Konoshchuk, D. M. Khmil, et al., *Theor. Exp. Chem*., **55,** 223-231 (2019), doi: 10.1007/s11237-019-09612-7.
95. N. V. Konoshchuk, O. Y. Posudievsky, V. G. Koshechko, et al., *Theor. Exp. Chem*., **55,** 316-323 (2019), doi: 10.1007/s11237-019-09623-4.
96. F. Mathies, H. Eggers, B. S. Richards, et al., *ACS Appl. Energy Mater*., **1,** 1834-1839 (2018), doi: 10.1021/acsaem.8b00222.
97. Y. Deng, E. Peng, Y. Shao, et al., *Energy Environ. Sci*., **8,** 1544-1550 (2015), doi: 10.1039/C4EE03907F.
98. F. Di Giacomo, S. Shanmugam, H. Fledderus, et al., *Sol. Energy Mater. Sol. Cells*, **181,** 53-59 (2018), doi: 10.1016/j.solmat.2017.11.010.
99. A. T. Barrows, A. J. Pearson, C. K. Kwak, et al., *Energy Environ. Sci*., **7,** 2944-2950 (2014), doi: 10.1039/c4ee01546k.
100. J. E. Bishop, T. J. Routledge, and D. G. Lidzey, *J. Phys. Chem. Lett*., **9,** 1977-1984 (2018), doi: 10.1021/acs.jpclett.8b00311.
101. J.-S. Yeo, Y.-H. Seo, C.-H. Jung, et al., *Nanoscale*, **11,** 890-900 (2019), doi: 10.1039/C8NR05698F.
102. C.-C. Zhang, Z.-K. Wang, M. Li, et al., *J. Mater. Chem. A*, **6,** 1161-1170 (2018), doi: 10.1039/C7TA08204E.
103. H. Zheng, G. Liu, C. Zhang, et al., *Sol. Energy*, **159,** 914-919 (2018), doi: 10.1016/j.solener.2017.09.039.
104. M. K. Nazeeruddin, A. Kay, I. Rodicio, et al., *J. Am. Chem. Soc*., **115,** 6382-6390 (1993), doi: 10.1021/ja00067a063.
105. M. Grätzel, *Acc. Chem. Res*., **42,** 1788-1798 (2009), doi: 10.1021/ar900141y.
106. A. Hagfeldt, G. Boschloo, L. Sun, et al., *Chem. Rev*., **110,** 6595-6663 (2010), doi: 10.1021/cr900356p.
107. L. E. Polander, A. Yella, B. F. E. Curchod, et al., *Angew. Chem*., **125,** 8893-8897 (2013), doi: 10.1002/ange.201304608.
108. T. Higashino and H. Imahori, *Dalton Trans*., **44,** 448-463 (2015), doi: 10.1039/C4DT02756F.
109. G. V. Bulavko and A. A. Ishchenko, *Russ. Chem. Rev*., **83,** 575 (2014), doi: 10.1070/RC2014v083n07ABEH004417.
110. L. Liu, Y. Kan, K. Gao, et al., *Adv. Mater*., **32,** 1907604 (2020), doi: 10.1002/adma.201907604.
111. M. Saliba, J. P. Correa-Baena, M. Grätzel, et al., *Angew. Chem. Int. Ed*., **57,** 2554-2569 (2018), doi: 10.1002/anie.201703226.
112. J. Prakash, A. Singh, G. Sathiyan, et al., *Mater. Today Energy*, **9,** 440-486 (2018), doi: 10.1016/j.mtener.2018.07.003.
113. G. Yang, H. Tao, P. Qin, et al., *J. Mater. Chem. A*, **4,** 3970-3990 (2016), doi: 10.1039/C5TA09011C.
114. K. Mahmood, S. Sarwar, and M. T. Mehran, *RSC Adv*., **7,** 17044-17062 (2017), doi: 10.1039/C7RA00002B.
115. M. Jiang, Q. Niu, X. Tang, et al., *Polymers*, **11,** 147 (2019), doi: 10.3390/polym11010147.
116. N. E. Courtier, J. M. Cave, J. M. Foster, et al., *Energy Environ. Sci*., **12,** 396-409 (2019), doi: 10.1039/C8EE01576G.
117. J. M. Ball, M. M. Lee, A. Hey, et al., *Energy Environ. Sci*., **6,** 1739-1743 (2013), doi: 10.1039/C3EE40810H.
118. D. Yang, R. Yang, K. Wang, et al., *Nat. Commun*., **9,** 1-11 (2018), doi: 10.1038/s41467-018-05760-x.
119. S. Pitchaiya, M. Natarajan, A. Santhanam, et al., *Arab. J. Chem*., **13,** 2526-2557 (2020), doi: 10.1016/j.arabjc.2018.06.006.
120. X. Liu, Z. Liu, B. Sun, et al., *Nano Energy*, **50,** 201-211 (2018), doi: 10.1016/j.nanoen.2018.05.031.
121. J. Tang, D. Jiao, L. Zhang, et al., *Sol. Energy*, **161,** 100-108 (2018), doi: 10.1016/j.solener.2017.12.045.
122. Q. Lin, Z. Wang, M. Young, et al., *Adv. Funct. Mater*., **27,** 1702485 (2017), doi: 10.1002/adftn.201702485.
123. Q. Lin, A. Armin, P. L. Burn, et al., *Nat. Photonics*, **9,** 687-694 (2015), doi: 10.1038/nphoton.2015.175.

124. B. Murali, M. I. Saidaminov, A. L. Abdelhady, et al., *J. Mater. Chem. C.*, **4,** 2545-2552 (2016), doi: 10.1039/C6TC00610H.
125. A. A. Ishchenko, I. L. Mushkalo, N. A. Derevyanko, et al., *J. Inf. Rec. Mater.,* **17,** 39-51 (1989).
126. A. A. Ishchenko, A. F. Dokukina, Z. A. Smirnova, et al., *Dokl. Akad. Nauk SSSR*., **284,** 1407-1411 (1985).
127. A. A. Ishchenko, *Russ. Chem. Rev*., **60,** 865 (1991), doi: 10.1070/RC1991v060n08ABEH001116.
128. A. I. Tolmachev, Y. L. Slominskii, and A. A. Ishchenko, *New Cyanine Dyes Absorbing in the NIR Region. Near-Infrared Dyes for High Technology Applications*, S. Daehne, U. Resch-Genger, and O. S. Wolfbeis (eds.), Springer, Dordrecht, Boston, London (1998), pp. 385-415, doi: 10.1007/978-94-011-5102-3_19.
129. A. A. Ishchenko, *Pure Appl. Chem*., **80,** 1525-1538 (2008), doi: 10.1351/pac200880071525.
130. A. V. Kulinich, N. A. Derevyanko, A. A. Ishchenko, et al., *Dyes Pigments*, **161,** 24-33 (2019), doi: 10.1016/j.dyepig.2018.09.031.
131. S.-M. Yoo, S. J. Yoon, J. A. Anta, et al., *Joule*, **3,** 2535-2549 (2019), doi: 10.1016/j.joule.2019.07.014.
132. N. Davidenko, I. Davidenko, A. Ishchenko, et al., *Appl. Opt.*, **51,** C48-C54 (2012), doi: 10.1364/AO.51.000C48.
133. I. V. Kurdiukova, A. V. Kulinich, and A. A. Ishchenko, *New J. Chem*., **36,** 1564-1567 (2012), doi: 10.1039/C2NJ40303J.
134. N. A. Derevyanko, A. A. Ishchenko, and A. V. Kulinich, *PCCP*, **22,** 2748-2762 (2020), doi: 10.1039/C9CP05827C.
135. V. N. Bliznyuk, J. Gasiorowski, A. A. Ishchenko, et al., *Org. Electron*., **15,** 1105-1112 (2014), doi: 10.1016/j.orgel.2014.03.003.
136. A. V. Kulinich, N. A. Derevyanko, and A. A. Ishchenko, *Russ. J. Gen. Chem*., **76,** 1441-1457 (2006), doi: 10.1134/S1070363206090167.
137. V. N. Bliznyuk, J. Gasiorowski, A. A. Ishchenko, et al., *Appl. Surf. Sci*., **389,** 419-427 (2016), doi: 10.1016/j.apsusc.2016.07.130.
138. J. S. Manser, M. I. Saidaminov, J. A. Christians, et al., *Acc. Chem. Res*., **49,** 330-338 (2016), doi: 10.1021/acs.accounts.5b00455.
139. Q. Fu, X. Tang, B. Huang, et al., *Adv. Sci.*, **5,** 1700387 (2018), doi: 10.1002/advs.201700387.
140. E. H. Jung, N. J. Jeon, E. Y. Park, et al., *Nature*, **567,** 511 (2019), doi: 10.1038/s41586-019-1036-3.
141. T.-H. Han, J.-W. Lee, C. Choi, et al., *Nat. Commun*., **10,** 520 (2019), doi: 10.1038/s41467-019-08455-z.
142. L. Zuo, H. Guo, D. W. deQuilettes, et al., *Sci. Adv*., **3,** e1700106 (2017), doi: 10.1126/sciadv.1700106.
143. Q. Jiang, Y. Zhao, X. Zhang, et al, *Nat. Photonics*, **13,** 460-466 (2019), doi: 10.1038/s41566-019-0398-2.
144. G. Niu, X. Guo, and L. Wang, *J. Mater. Chem. A*, **3,** 8970-8980 (2015), doi: 10.1039/C4TA04994B.
145. Q. Wang, N. Phung, D. Di Girolamo, et al., *Energy Environ. Sci*., **12,** 865-886 (2019), doi: 10.1039/C8EE02852D.
146. I. Hwang, I. Jeong, J. Lee, et al., *ACS Appl. Mater. Interfaces*, **7,** 17330-17336 (2015), doi: 10.1021/acsami.5b04490.
147. F. U. Kosasih and C. Ducati, *Nano Energy*, **47,** 243-256 (2018), doi: 10.1016/j.nanoen.2018.02.055.
148. F. Matteocci, S. Razza, F. Di Giacomo, et al., *PCCP*, **16,** 3918-3923 (2014), doi: 10.1039/C3CP55313B.
149. M. Asghar, J. Zhang, H. Wang, et al., *Renew. Sust. Energ. Rev*., **77,** 131-146 (2017), doi: 10.1016/j.rser.2017.04.003.
150. A. Kitai, *Principles of Solar Cells, LEDs and Related Devices. The Role of the PN Junction*, John Wiley & Sons Ltd., Chichester, UK (2019) ISBN: 9781119451020.
151. J. S. Shaikh, N. S. Shaikh, A. D. Sheikh, et al., *Mater. Des*., **136,** 54-80 (2017), doi: 10.1016/j.matdes.2017.09.037.
152. U. Mehmood, A. Al-Ahmed, M. Afzaal, et al., *Renew. Sust. Energ. Rev*., **78,** 1-14 (2017), doi: 10.1016/i.rser.2017.04.105.
153. J. A. Christians, P. A. Miranda Herrera, and P. V. Kamat, *J. Am. Chem. Soc*., **137,** 1530-1538 (2015), doi: 10.1021/ja511132a.
154. I. Deretzis, E. Smecca, G. Mannino, et al., *J. Phys. Chem. Lett*., **9,** 3000-3007 (2018), doi: 10.1021/acs.jpclett.8b00120.
155. W. Huang, J. S. Manser, P. V. Kamat, et al., *Chem. Mater*., **28,** 303-311 (2016), doi: 10.1021/acs.chemmater.5b04122.
156. R. S. Sanchez, V. Gonzalez-Pedro, J.-W. Lee, et al., *J. Phys. Chem. Lett*., **5,** 2357-363 (2014), doi: 10.1021/jz5011187.
157. E. L. Unger, E. T. Hoke, C. D. Bailie, et al., *Energy Environ. Sci.*, **7,** 3690-3698 (2014), doi: 10.1039/C4EE02465F.
158. C. A. Omondi, Dr. rer. nat., *Technischen Universitat Berlin,* Berlin, 157 (2018).
159. D. Bryant, N. Aristidou, S. Pont, et al., *Energy Environ. Sci*., **9,** 1655-1660 (2016), doi: 10.1039/C6EE00409A.
160. N. H. Nickel, F. Lang, V. V. Brus, et al., *Adv. Electron. Mater*., **3,** 1700158 (2017), doi: 10.1002/aelm.201700158.

161. A. Dey, A. Dhar, S. Roy, et al., *Mater. Today: Proc.*, **4,** 12651-12656 (2017), doi: 10.1016/j.matpr.2017.10.077.
162. A. Pisoni, J. Jacimovic, O. S. Barisic, et al., *J. Phys. Chem. Lett*., **5,** 2488-2492 (2014), doi: 10.1021/jz5012109.
163. B. Conings, J. Drijkoningen, N. Gauquelin, et al., *Adv. Energy Mater*., **5,** 1500477 (2015), doi: 10.1002/aenm.201500477.
164. H. S. Kim, J. Y. Seo, and N. G. Park, *ChemSusChem*., **9,** 2528-2540 (2016), doi: 10.1002/cssc.201600915.
165. D. W. Boukhvalov, I. S. Zhidkov, A. F. Akbulatov, et al., *J. Phys. Chem. A*, **124,** 135-140 (2019), doi: 10.1021/acs.jpca.9b09653.
166. G. E. Eperon, S. D. Stranks, C. Menelaou, et al., *Energy Environ. Sci*., **7,** 982-988 (2014), doi: 10.1039/C3EE43822H.
167. S. N. Habisreutinger, T. Leijtens, G. E. Eperon, et al., *Nano Lett*., **14,** 5561-5568 (2014), doi: 10.1021/nl501982b.
168. N. Arora, M. I. Dar, A. Hinderhofer, et al., *Science*, **358,** 768-771 (2017), doi: 10.1126/science.aam5655.
169. B. Roose, C. M. Johansen, K. Dupraz, et al., *J. Mater. Chem. A*, **6,** 1850-1857 (2018), doi: 10.1039/C7TA07663K.
170. M. Zhu, F. Hao, L. Ma, et al., *ACS Energy Lett*., **1,** 469-473 (2016), doi: 10.1021/acsenergylett.6b00249.
171. K. Wojciechowski, T. Leijtens, S. Siprova, et al., *J. Phys. Chem. Lett*., **6,** 2399-2405 (2015), doi: 10.1021/acs.jpclett.5b00902.
172. E. J. Juarez-Perez, L. K. Ono, M. Maeda, et al., *J. Mater. Chem. A*., **6,** 9604-9612 (2018), doi: 10.1039/C8TA03501F.
173. W. Nie, J.-C. Blancon, A. J. Neukirch, et al., *Nat. Commun*., **7,** 1-9 (2016), doi: 10.1038/ncomms11574.
174. X. Tang, M. Brandl, B. May, et al., *J. Mater. Chem. A*, **4,** 15896-15903 (2016), doi: 10.1039/C6TA06497C.
175. S. Xiong, J. Song, J. Yang, et al., *Solar RRL*, **4,** 1900529 (2020), doi: 10.1002/solr.201900529.
176. X. Zheng, B. Chen, J. Dai, et al., *Nat. Energy*, **2,** 1-9 (2017), doi: 10.1038/nenergy.2017.102.
177. H. Zhang, M. K. Nazeeruddin, and W. C. H. Choy, *Adv. Mater*., **31,** 1805702 (2019), doi: 10.1002/adma.201805702.
178. G. J. A. Wetzelaer, M. Scheepers, A. M. Sempere, et al., *Adv. Mater*., **27,** 1837-1841 (2015), doi: 10.1002/adma.201405372.
179. T. Zhao, C.-C. Chueh, Q. Chen, et al., *ACS Energy Lett*., **1,** 757-763 (2016), doi: 10.1021/acsenergylett.6b00327.
180. J. Yang, Q. Hong, Z. Yuan, et al., *Adv. Opt. Mater*., **6,** 1800262 (2018), doi: 10.1002/adom.201800262.
181. J. Yang, X. Liu, Y. Zhang, et al., *Nano Energy*, **54.** 218-226 (2018), doi: 10.1016/j.nanoen.2018.10.011.
182. R.-P. Xu, Y.-Q. Li, T.-Y. Jin, et al., *ACS Appl. Mater. Interfaces*, **10,** 6737-6746 (2018), doi: 10.1021/acsami.7b18389.
183. S. Wang, Z. Li, Y. Zhang, et al., *Adv. Funct. Mater*., **29,** 1900417 (2019), doi: 10.1002/adfm.201900417.
184. F. Cai, Y. Yan, J. Yao, et al., *Adv. Funct. Mater*., **28,** 1801985 (2018), doi: 10.1002/adfm.201801985.
185. H. L. Hsu, H. T. Hsiao, T. Y. Juang, et al., *Adv. Energy Mater*., **8,** 1802323 (2018), doi: 10.1002/aenm.201802323.
186. T.-H. Han, J.-W. Lee, C. Choi, et al., *Nat. Commun*., **10,** 1-10 (2019), doi: 10.1038/s41467-019-08455-z.
187. W.-Q. Wu, Z. Yang, P. N. Rudd, et al., *Sci. Adv*., **5,** eaav8925 (2019), doi: 10.1126/sciadv.aav8925.
188. T. Wu, Y. Wang, Z. Dai, et al., *Adv. Mater*., **31,** 1900605 (2019), doi: 10.1002/adma.201900605.
189. T. Wu, Y. Wang, X. Li, et al., *Adv. Energy Mater.*, **9,** 1803766 (2019), doi: 10.1002/aenm.201803766.
190. Y. Chen, N. Li, L.Wang, et al., *Nat. Commun*., **10,** 1-10 (2019), doi: 10.1038/s41467-019-09093-1.
191. L. Zuo, H. Guo, D. W. deQuilettes, et al., *Sci. Adv*., **3,** e1700106 (2017), doi: 10.1126/sciadv.1700106.
192. A. Nitti, M. Signorile, M. Boiocchi, et al., *J. Org. Chem*., **81,** 11035-11042 (2016), doi: 10.1021/acs.joc.6b01922.
193. M. Zhang, M. Tai, X. Li, et al., *Solar RRL*, **3,** 1900345 (2019), doi: 10.1002/solr.201900345.
194. S. Yang, Z. Guo, L. Gao, et al., *Solar RRL*, **3,** 1900212 (2019), doi: 10.1002/solr.201900212.
195. X. Li, C. C. Chen, M. Cai, et al., *Adv. Energy Mater*., **8,** 1800715 (2018), doi: 10.1002/aenm.201800715.
196. S. Tsarev, T. S. Dubinina, S. Y. Luchkin, et al., *J. Phys. Chem. C*, **124,** 1872-1877 (2019), doi: 10.1021/acs.jpcc.9b10709.
197. F. Bella, G. Griffini, J. -P. Correa-Baena, et al., *Science*, **354,** 203-206 (2016), doi: 10.1126/science.aah4046.
198. V. N. Bliznyuk, A. F. Seliman, A. A. Ishchenko, et al., *ACS Appl. Mater. Interfaces*, **8**,12843-12851 (2016), doi: 10.1021/acsami.6b02719.
199. A. A. Ishchenko, F. G. Kramarenko, A. G. Maydannic, et al., *J. Inf. Rec. Mater*., **19,** 207-219 (1991).
200. A. A. Ishchenko and G. P. Grabchuk, *Theor. Exp. Chem*., **45,** 143-167 (2009), doi: 10.1007/s11237-009-9078-5.
201. A. A. Ishchenko, *Theor. Exp. Chem*., **34,** 191-210 (1998), doi: 10.1007/BF02523249.
202. A. V. Kulinich, N. A. Derevyanko, A. A. Ishchenko, et al., *J. Photochem. Photobiol. A, Chem*., **197,** 40-49 (2008), doi: 10.1016/j.jphotochem.2007.12.003.

203. A. V. Kulinich and A. A. Ishchenko, *J. Appl. Spectrosc*., **86,** 35-42 (2019), doi: 10.1007/s10812-019-00777-6.
204. W. Li, W. Zhang, S. Van Reenen, et al., *Energy Environ. Sci*., **9,** 490-498 (2016), doi: 10.1039/C5EE03522H.
205. J. C. V. P. Moura, A. M. F. Oliveira-Campos, and J. Griffiths, *Dyes Pigments*, **33,** 173-196 (1997), doi: 10.1016/S0143-7208(96)00050-2.
206. A. A. Ishchenko, *Polym. Adv. Technol*., **13,** 744-752 (2002), doi: 10.1002/pat.269.
207. W. Li, T. Mori, and T. Michinobu, *MRS Commun*., **8,** 1244-1253 (2018), doi: 10.1557/mrc.2018.119.
208. D. Y. Park, H. R. Byun, H. Kim, et al., *J. Kor. Phys. Soc*., **73,** 1787-1793 (2018), doi: 10.3938/jkps.73.1787.
209. S. Valero, S. Collavini, S. F. Volker, et al., *Macromolecules*, **52,** 2243-2254 (2019), doi: 10.1021/acs.macromol.9b00165.
210. Y. Zhang, P. Heng, H. Su, et al., *Chem. Rec*., **19,** 938-946 (2019), doi: 10.1002/tcr.201800150.
211. N. J. Jeon, H. Na, E. H. Jung, et al., *Nature Energy*, **3,** 682-689 (2018), doi: 10.1038/s41560-018-0200-6.
212. Y. Zhang, L. Wang, L. Mao, et al., *Spectrochim. Acta A*, **228,** 117808 (2020), doi: 10.1016/j.saa.2019.117808.
213. S. Ding, S. Li, Q. Sun, et al., *J. Mater. Chem. C*, **7,** 5686-5694. (2019) doi: 10.1039/C9TC00064J.
214. X. Zhao, C. Yao, T. Liu, et al., *Adv. Mater*., **31,** 1904494 (2019), doi: 10.1002/adma.201904494.
215. J. H. Kang, Y. J. Park, Y. Khan, et al., *Dyes Pigments*, **182,** 108634 (2020), doi: 10.1016/j.dyepig.2020.108634.
216. M. Hosseinnezhad, *J. Electron. Mater*., **48,** 5403-5408 (2019), doi: 10.1007/s11664-019-07272-w.
217. M. H. Kumar, S. Dharani, W. L. Leong, et al., *Adv. Mater*., **26,** 7122-7127 (2014), doi: 10.1002/adma.201401991.
218. Y. Fu, F. Meng, M. B. Rowley, et al., *J. Am. Chem. Soc*., **137,** 5810-5818 (2015), doi: 10.1021/jacs.5b02651.
219. C. B. Murray, C. R. Kagan, and M. G. Bawendi, *Annu. Rev. Mater. Sci*., **30,** 545-610 (2000), doi: 10.1146/annurev.matsci.30.1.545.
220. L. C. Schmidt, A. Pertegas, S. Gonzalez-Carrero, et al., *J. Am. Chem. Soc*., **136,** 850-853 (2014), doi: 10.1021/ja4109209.
221. S. Gonzalez-Carrero, R. E. Galian, and J. Perez-Prieto, *J. Mater. Chem. A*, **3,** 9187-9193 (2015), doi: 10.1039/C4TA05878J.
222. L. Protesescu, S. Yakunin, M. I. Bodnarchuk, et al., *Nano Lett*., **15,** 3692-3696 (2015).
223. S. van Reenen, M. Kemerink, and H. J. Snaith, *J. Phys. Chem. Lett*., **6,** 3808-3814 (2015), doi: 10.1021/acs.jpclett.5b01645.
224. P. Calado, A. M. Telford, D. Bryant, et al., *Nat. Commun*., **7,** 1-10 (2016), doi: 10.1038/ncomms13831.
225. V. Adinolfi, M. Yuan, R. Comin, et al., *Adv. Mater*., **28,** 3406-3410 (2016), doi: 10.1002/adma.201505162.
226. O. I. V'yunov, A. G. Belous, S. D. Kobylianska, et al., *Nanoscale Res. Lett*., **13,** 98 (2018), doi: 10.1186/s11671-018-2509-2.
227. W. Huang, J. S. Manser, P. V. Kamat, et al., *Chem. Mater*., **28,** 303-311 (2016), doi: 10.1021/acs.chemmater.5b04122.
228. O. G. Vendyk, S. P. Zubko, and M. A. Nikolskyi, *Zh. Tekh. Fiz.*, **69,** 1-7 (1999).
229. S. S. Gevorgian, T. Martinsson, P. L. J. Linner, et al., *IEEE Trans. Microw. Theory Technol*., **44,** 896-904 (1996), doi: 10.1109/22.506449.
230. N. Onoda-Yamamuro, T. Matsuo, and H. Suga, *J. Phys. Chem. Solids*, **53,** 935-939 (1992), doi: 10.1016/0022-3697(92)90121-S.
231. G. Grancini, C. Roldan-Carmona, I. Zimmermann, et al., *Nat. Commun*., **8,** 1-8 (2017), doi: 10.1038/ncomms15684.
232. M. Lyu, J. H. Yun, P. Chen, et al., *Adv. Energy Mater*., **7,** 1602512 (2017), doi: 10.1002/aenm.201602512.
233. J. Chen, S. -G. Kim, X. Ren, et al., *J. Mater. Chem. A.*, **7,** 4977-4987 (2019), doi: 10.1039/c8ta11977e.
234. Editorial article, *Nature Energy*, **4,** 1-1 (2019), doi: 10.1038/s41560-018-0323-9.
235. Solar Power Has Big Limitations. This Wonder Material Could Change That, (2016) URL: (accessed 24 November, 2020).
236. W. Tress, N. Marinova, T. Moehl, et al., *Energy Environ. Sci*., **8,** 995-1004 (2015), doi: 10.1039/C4EE03664F.
237. F. Huang, M. Li, P. Siffalovic, et al., *Energy Environ. Sci*., **12,** 518-549 (2019), doi: 10.1039/C8EE03025A.
238. Oxford PV Perovskite Solar Cell Achieves 28% Efficiency (2018), https://www.oxfordpv.com/news/oxford-pv-perovskite-solar-cell-achieves-28-efficiency (accessed 15 May, 2020).
239. Toshiba Develops 703 cm^2 Film-Based Perovskite Photovoltaic Module with a 11.7 Percent Power Conversion Efficiency (2018), https://www.cdrinfo.com/Sections/News/Print.aspx?NewsId=70171 (accessed 15 May, 2020).

240. Saule Technologies' Perovskite-Based Solar Panels Headed for Commercial Implementation by Building Company Skanska (2018), https://www.perovskite-info.com/saule-technologies-perovskite-based-solar-panels-headed-comercial-implementation-building-company (accessed 15 May, 2020).
241. N. K. Ibrayev, E. V. Seliverstova, A. A. Ishchenko, et al., *J. Photochem. Photobiol. A. Chem*., **346,** 570-575 (2017), doi: 10.1016/j.jphotochem.2017.06.029.
242. A. V. Kulinich and A. A. Ishchenko, *Russ. Chem. Rev*., **78,** 141 (2009), doi: 10.1070/RC2009v078n02ABEH003900.
243. N. A. Davidenko, I. I. Davidenko, A. A. Ishchenko, et al., *J. Appl. Spectrosc*., **86,** 578-583 (2019), doi: 10.1007/s10812-019-00862-w.
244. G. V. Bulavko, N. A. Davidenko, A. G. Shkavro, et al., *Funct. Mater. Lett*., **10,** 1750007(1-5) (2017), doi: 10.1142/S1793604717500072.
245. A. A. Ishchenko, A. V. Kulinich, S. L. Bondarev, et al., *Spectrochim. Acta A*, **190,** 332-335 (2018), doi: 10.1016/j.saa.2017.09.054.
246. N. Graβler, S. Wolf, F. Holzmuller, et al., *Eur. J. Org. Chem*., **2019,** 845-851 (2019), doi: 10.1002/ejoc.201801512.
247. F. Wurthner, T. E. Kaiser, and C. R. Saha-Moller, *Angew. Chem. Int. Ed*., **50,** 3376-3410 (2011), doi: 10.1002/anie.201002307.
248. S. Valleau, A. Eisfeld, and A. Aspuru-Guzik, *J. Chem. Phys.*, **137,** 224103 (2012), doi: 10.1063/1.4732122.
249. S. Harazi, O. Kapon, A. Sharoni, et al., *J. Phys. Chem. C*, **123,** 19087-19093 (2019), doi: 10.1021/acs.jpcc.9b01116.
250. C. C. L. Cheung, G. Ma, K. Karatasos, et al., *Nanotheranostics*, **4,** 91 (2020), doi: 10.7150/ntno.41737.
251. C. -A. Shen and F. Wurthner, *Chem. Commun*., **56,** 9878-9881 (2020), doi: 10.1039/D0CC03686B.
252. Y. Kitahama, M. Funaoka, and Y. Ozaki, *J. Phys. Chem. C*, **123,** 18001-18006 (2019), doi: 10.1021/acs.jpcc.9b05626.
253. Y. Wang and T. Ding, *Nanoscale*, **11,** 10589-10594 (2019), doi: 10.1039/c9nr03725j.
254. E. V. Seliverstova, D. A. Temirbayeva, N. K. Ibrayev, et al., *Theor. Exp. Chem*., **55,** 115-124 (2019), doi: 10.1007/s11237-019-09602-9.
255. N. Ibrayev, A. Ishchenko, D. Afanasyev, et al., *Appl. Phys. B*, **125,** 182 (2019), doi: 10.1007/s00340-019-7292-y.
256. R. S. Moakhar, S. Gholipour, S. Masudy-Panah, et al., *Adv. Sci*., **7,** 1902448 (1-19) (2020), doi: 10.1002/advs.201902448.